© 2018. Published by The Company of Biologists Ltd | Development (2018) 145, dev159640. doi:10.1242/dev.159640

RESEARCH ARTICLE

Phosphorylation states change Otx2 activity for cell proliferation and patterning in the *Xenopus* embryo

Yumeko Satou[1], Kohei Minami[1], Erina Hosono[1], Hajime Okada[1], Yuuri Yasuoka[1,2], Takashi Shibano[1,*], Toshiaki Tanaka[3] and Masanori Taira[1,‡]

ABSTRACT

The homeodomain transcription factor Otx2 has essential roles in head and eye formation via the negative and positive regulation of its target genes, but it remains elusive how this dual activity of Otx2 affects cellular functions. In the current study, we first demonstrated that both exogenous and endogenous Otx2 are phosphorylated at multiple sites. Using *Xenopus* embryos, we identified three possible cyclin-dependent kinase (Cdk) sites and one Akt site, and analyzed the biological activities of phosphomimetic (4E) and nonphosphorylatable (4A) mutants for those sites. In the neuroectoderm, the 4E but not the 4A mutant downregulated the Cdk inhibitor gene *p27xic1* (*cdknx*) and posterior genes, and promoted cell proliferation, possibly forming a positive-feedback loop consisting of Cdk, Otx2 and p27xic1 for cell proliferation, together with anteriorization. Conversely, the 4A mutant functioned as an activator on its own and upregulated the expression of eye marker genes, resulting in enlarged eyes. Consistent with these results, the interaction of Otx2 with the corepressor Tle1 is suggested to be phosphorylation dependent. These data suggest that Otx2 orchestrates cell proliferation, anteroposterior patterning and eye formation via its phosphorylation state.

KEY WORDS: Otx2, Anteroposterior patterning, Cell proliferation, Eye formation, Post-translational modification

INTRODUCTION

Gene regulation by transcription factors (TFs) is fundamental to cellular and developmental regulatory processes, and some TFs are likely to be regulated by various modifications, including phosphorylation, forming regulatory axes or loops to drive a tissue-specific program of gene expression (Spitz and Furlong, 2012). However, it is not fully understood how modifications of TFs orchestrate regulation in cellular or developmental processes.

The homeobox gene *orthodenticle* (*otd*), which encodes the bicoid-type homeodomain TF, is required for the formation of the anterior portion of the head in bilaterians (Holland et al., 2013). *otx2* is a vertebrate homolog of *otd*, and is required for head and eye development (Blitz and Cho, 1995; Matsuo et al., 1995; Suda et al., 2009; Andreazzoli et al., 1997; Isaacs et al., 1999; Pannese et al., 1995). The expression of *otx2* begins in the anterior neuroectoderm, which further develops into the forebrain and midbrain, and the gene has an essential role in anteroposterior patterning to prevent caudalization by Meis3 and Gbx2 (Agoston and Schulte, 2009; Katahira et al., 2000). In eye development, Otx2 upregulates an eye field-specific gene, *rax*, in the center of the *otx2*-expressing domain at the gastrula stage (Danno et al., 2008); in turn, Rax downregulates *otx2* to discriminate the eye field from the diencephalon (Andreazzoli et al., 1999; Zuber, 2010). During later eye development, expression of *otx2* restarts in the developing optic vesicle (Viczian et al., 2003; Martinez-Morales et al., 2001), and is involved in the specification of presumptive neural retina (*pax6*-positive cells) from the optic stalk (*pax2*-positive cells) in mice (Martinez-Morales et al., 2001). After retinal specification, *otx2* expression becomes restricted to postmitotic retinal progenitors, and determines bipolar cell fate (Brzezinski and Reh, 2015). Thus, we are gradually beginning to understand the role of Otx2 in head and eye formation.

Otx2 has both transactivation and transrepression activities in the regulation of downstream target genes. It has a transactivation domain in the C-terminal region (Gammill and Sive, 2001) and directly upregulates a cement gland marker, *xcg1* (*muc2*) in *Xenopus* (Gammill and Sive, 1997). Otx2 also has a repression domain with a motif of SIWSPAS, which belongs to engrailed homology region 1 (eh1) (Heimbucher et al., 2007). This domain is conserved in vertebrate Otx family proteins and interacts with the co-repressor TLE/Groucho (Heimbucher et al., 2007). With this domain, Otx2 functions as a repressor that inhibits the posterior gene *gbx2* to form the midbrain–hindbrain boundary (MHB) (Nakamura et al., 2005). Furthermore, genome-wide analysis of chromatin immunoprecipitation (ChIP) sequencing using *Xenopus tropicalis* gastrula embryos showed that Otx2 cooperates with the transcriptional activator Lim1 (Lhx1) to bind specific *cis*-regulatory modules (CRMs) to activate anterior genes in the head organizer, whereas Otx2 cooperates with the repressor Goosecoid (Gsc) to inhibit nonhead-organizer genes (Yasuoka et al., 2014). Thus, both the transactivation and transrepression activities of Otx2 are important for regionalization and tissue patterning and function during embryogenesis.

Recently, several reports have shown that Otx2 directly influences both cell proliferation and differentiation. In mice, aberrant expression of Otx2 in the hindbrain induces the ectopic proliferation of neural progenitor cells (Wortham et al., 2012), and overexpression of Otx2 causes proliferation of dopaminergic progenitors in the ventral mesencephalon (Omodei et al., 2008; Vernay et al., 2005). In addition, in a medulloblastoma cell line, Otx2 upregulates cell cycle-positive regulator genes, such as *ccnd3* (cyclin D3), and downregulates cell cycle-negative regulator genes,

[1]Department of Biological Sciences, Graduate School of Science, University of Tokyo, Hongo 7-3-1, Bunkyo-ku, Tokyo 113-0033, Japan. [2]Marine Genomics Unit, Okinawa Institute of Science and Technology Graduate University, 1919-1 Tancha, Onna-son, Okinawa 904-0495, Japan. [3]Department of Life Science and Technology, Tokyo Institute of Technology, 4259 Nagatsuta, Midori-ku, Yokohama 226-8501, Japan.
*Present address: Department of Oncology-Pathology, Karolinska Institutet, CCK R8:04, Karolinska Universitetssjukhuset, 17176 Stockholm, Sweden.

‡Author for correspondence (m_taira@bs.s.u-tokyo.ac.jp)

Y.S., 0000-0001-8666-9327; K.M., 0000-0003-4247-0310; H.O., 0000-0002-3204-3633; M.T., 0000-0003-0981-4927

Received 28 September 2017; Accepted 1 February 2018

Development (2018) 145, dev159640. doi:10.1242/dev.159640

including *p27*, and differentiation-specific genes, such as *neuroD* (Bunt et al., 2012). Thus, Otx2 is likely to be involved in both proliferation and differentiation. However, the molecular mechanism of how Otx2 coordinates cell proliferation and differentiation by negatively and positively regulating direct target genes remains unknown.

Here, we show that Otx2 is phosphorylated, which confers transrepression activity; if Otx2 is not phosphorylated then it can only act as a transactivator. Functional analyses using phosphomimetic or nonphosphorylatable Otx2 mutants suggest that phosphorylated Otx2 represses the cyclin-dependent kinase (Cdk) inhibitor gene *p27xic1* (*cdknx*) and the posterior gene *gbx2* to promote cell proliferation and anteriorize the neuroectoderm, respectively, whereas unphosphorylated Otx2 enhances the formation of the eye field and later the retina in the optic stalk. Thus, our data provide a new model in which the post-translational regulation of Otx2 results in versatile functions of this protein, including cell proliferation- and differentiation-orientated activities.

RESULTS

Phosphorylation of exogenous Otx2

During western blot analyses of exogenous Otx2 in the *Xenopus laevis* embryo (Sudou et al., 2012), we noticed several bands of Otx2 that were migrating more slowly than an *in vitro* translated product. Similarly, several previous studies using western blots showed multiple bands of exogenous mouse Otx2 in transfected cultured cells (Mallamaci et al., 1996) and endogenous Otx2 in the mouse embryo (Boyl et al., 2001), although these have yet to be characterized. To evaluate the modification of Otx2, we constructed N-terminally Myc-tagged full-length Otx2 (Myc-Otx2FL) and its deletion constructs (Myc-Otx2HD, ΔAD, AD and ΔRD) (Fig. 1A), and expressed them by mRNA injection into *X. laevis* embryos for western blot analysis. The Myc-Otx2FL and ΔAD but not ΔRD, HD or AD constructs clearly showed several slowly migrating bands (magenta arrowheads in Fig. 1B and Fig. S1A), compared with the *in vitro* translated product (blue arrowheads in Fig. 1B and Fig. S1A). These data suggest that modification mainly occurs in the region of amino acid positions 96-184 (Fig. 1A).

The amino acid sequence from position 96 to 184 indicated possible phosphorylation sites for Cdk (S*/T*-P or S*/T*-P-X-R/K; asterisk indicates phosphorylatable residues), mitogen-activated protein kinase (MAPK), casein kinase (S*/T*-X_{0-2}-D/E/S^{P}_{1-3}; S^{P}, primary phosphorylatable serine residue), and Akt kinase (R/K-X_{2}-S*/T*) (Fig. 1C). Mouse Otx2 reportedly has an Akt phosphorylation site at S115 (the corresponding site of *X. laevis* Otx2 is T115; Fig. S2), according to the database for the prediction of phosphorylation sites (see Materials and Methods). To identify modification sites, we first examined seven serine residues (S116, S122, S123, S132, S153, S158 and S161) and one threonine (T115) by introducing point mutations in Myc-Otx2ΔAD. Replacement of a single serine with alanine revealed that S116A, S132A and S158A constructs eliminated the uppermost band and increased the lower bands compared with the wild type (WT) and other mutants (S122A, S123A, S153A and S161A) (Fig. S1B,C). Furthermore, a triple-alanine mutant of Myc-Otx2ΔAD for S116, S132 and S158 (named ΔAD-3A) showed no slowly migrating bands (Fig. 1D, lane 3). These data suggest that S116, S132 and S158, which have the S-P consensus motif for Cdk and MAPK, are responsible for multiple shifted bands (up to seven bands by combinations of three sites) of Myc-Otx2. To examine this suggestion, embryonic lysates expressing Myc-Otx2 constructs were treated with λ-protein phosphatase (λ-PP). λ-PP treatment removed all of the modified bands of Myc-Otx2ΔAD (Fig. 1D, lanes 1 and 2) and did not change the band of ΔAD-3A itself (Fig. 1D, lanes 3 and 4), suggesting that slowly migrating bands of Myc-Otx2ΔAD were caused by phosphorylation at S116, S132 and S158. The same experiment was performed with Myc-Otx2FL, with similar results, whereby all modified bands of Myc-Otx2FL were removed by λ-PP treatment except for a weak band that is shifted (Fig. S1D). Consistently, Myc-Otx2FL-3A had only a single weak shifted band, which was not removed with λ-PP (Fig. S1D, orange arrowhead), suggesting another distinct modification site around the activation domain.

We next asked whether T115 of *Xenopus* Otx2 is an Akt phosphorylation site, although we did not detect a shifted band in the Otx2 mutant 3A (ΔAD-3A) using western blotting (Fig. 1D, lanes 3 and 4). In addition, there was no difference in band positions between ΔAD-3A (remaining T115) and ΔAD-4A (alanine mutation at T115 in addition to 3A) regardless of λ-PP (Fig. 1D, lanes 3-6). However, it was still possible that phosphorylation at T115 either did not cause a band shift in ΔAD-3A in western blotting or was inhibited by alanine mutations at the three sites including S116 next to T115. Therefore, we performed immunoprecipitation (IP)-western blot assays using anti-Phospho-Akt Substrate antibody, which recognizes the R-X-X-S^{P}/T^{P} motif (S^{P}/T^{P}, phosphorylated residues). Myc-Otx2ΔAD in embryonic lysates was immunoprecipitated with anti-Myc antibody and then subjected to western blotting with anti-Phospho-Akt Substrate antibody. A band was detected with mutant ΔAD-3A but not with ΔAD-4A (Fig. 1E, upper panel, lanes 2 and 3), suggesting T115 as an Akt site. Thus, we identified four possible phosphorylation sites for Akt (T115) and Cdk/MAPK (S116, S132 and S158) in Otx2, and these sites are well conserved in vertebrate Otx2 as well as an Otx2 paralog/ohnolog, Otx5/Crx (Fig. S2).

Phosphorylation of endogenous Otx2

Although it is important to determine whether endogenous Otx2 is phosphorylated, no antibodies against phosphorylated sites of Otx2 are available. As far as we know, there is no report on detecting the phosphorylation of TFs expressed region specifically and endogenously in *Xenopus* embryos, such as Otx2, as evidenced by band shift in western blotting, possibly because of the limited amounts of such TFs in the whole embryo. Therefore, we first estimated the sensitivity of detection using a diluted series of *otx2* mRNA injected into *Xenopus* embryos. Modified bands of full-length Otx2 without a Myc-tag (Otx2FL) were clearly detected when >200 pg *otx2FL* mRNA was exogenously injected per embryo (Fig. S3). Based on RNA-seq data from *X. tropicalis* (Owens et al., 2016), the amount of *otx2* mRNA was estimated to be in the order of 1 pg per embryo at the neurula stage. Therefore, we predicted that endogenous Otx2 can be detected by western blotting of samples from more than 200 *X. tropicalis* embryos. As expected, we successfully detected multiple bands of endogenous Otx2 protein immunoprecipitated from lysates of approximately 800 *X. laevis* neurula embryos in total, and the upper bands were reduced by λ-PP treatment (Fig. 1F, left). Similarly, shifted bands of exogenous Otx2FL were detected, and were abolished by λ-PP treatment (Fig. 1F, right). Thus, endogenous Otx2 is phosphorylated, although the intensities of phosphorylated bands of endogenous Otx2 appeared to be lower than those of exogenous Otx2 (see Discussion).

Phosphorylation of Otx2 depends on Cdk activity

Given that S116, S132 and S158 sites have the S-P motif (Fig. 1C), we speculated that MAPK or cyclin/Cdk complexes phosphorylate

Development (2018) 145, dev159640. doi:10.1242/dev.159640

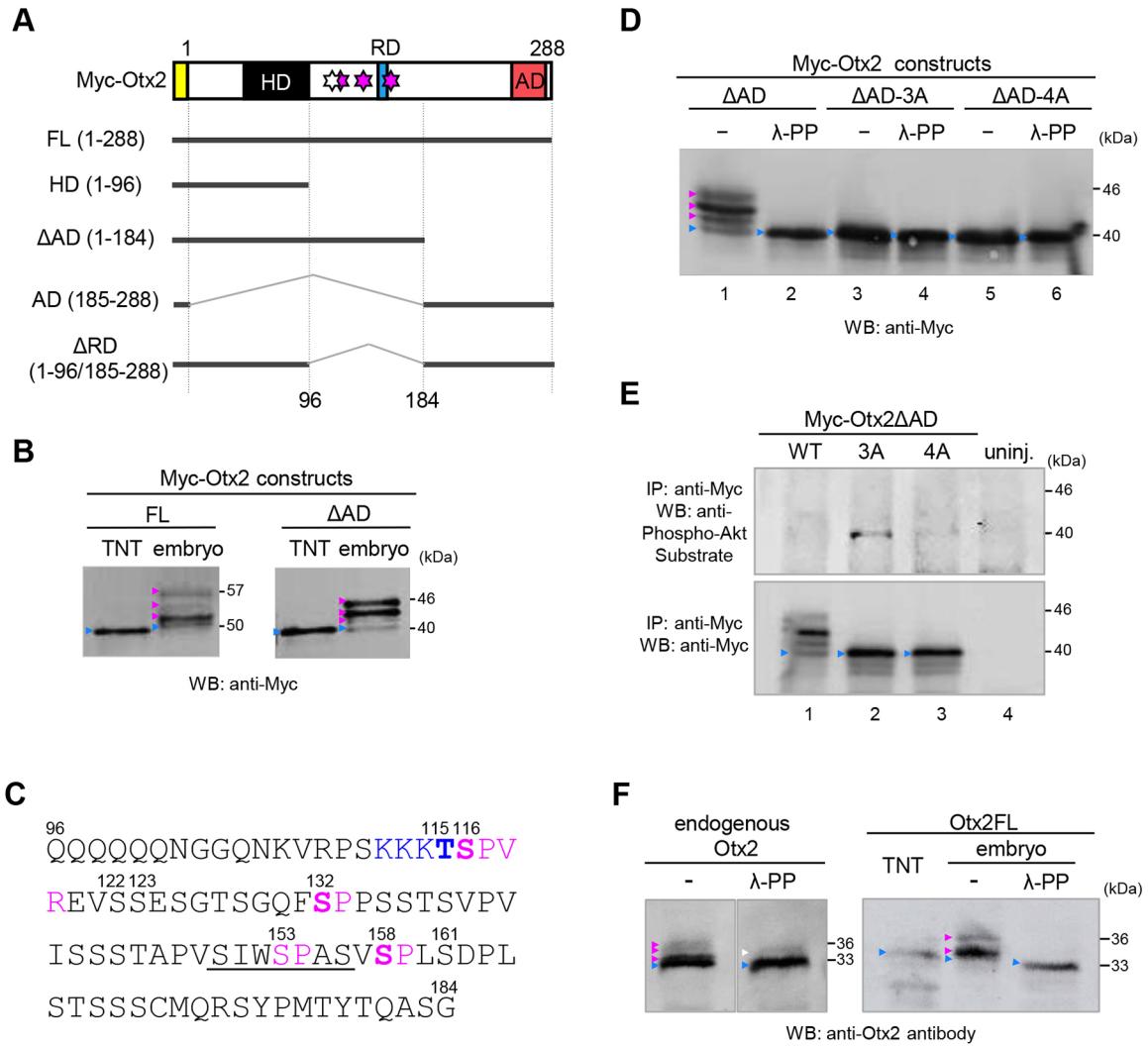

Fig. 1. Exogenous and endogenous Otx2 is phosphorylated. (A) Schematic structures of Myc-Otx2 and deletion constructs. HD, homeodomain; RD, repression domain; AD, activation domain; yellow box, Myc-tag; white star, Akt site; pink stars, Cdk sites. FL and deletion constructs are indicated by thick lines and positions of amino acid residues. (B) Western blotting of Myc-FL and Myc-ΔAD. TNT, *in vitro* translational products; embryo, lysate from *Xenopus* gastrula embryos expressing constructs as indicated. (C) Amino acid sequence of Otx2 from position 96 to 184. Numbers, position of amino acid; underline, repression domain; magenta, putative Cdk site; blue, putative Akt site; bold, possible phosphorylation sites identified in this study. (D) Western blotting of Myc-Otx2ΔAD constructs, WT, 3A and 4A. Lysates were treated with or without λ-PP. (E) IP-western assay for phospho-Akt sites. Myc-Otx2ΔAD was immunoprecipitated with anti-Myc antibody and subjected to western blotting with the anti-Phospho-Akt substrate antibody (upper) or anti-Myc antibody (lower). uninj. indicates uninjected control. The reasons why no clear band was detected in WT (lane 1) might be that: (i) phospho-Akt signals were dispersed in several shifted bands caused by phosphorylation at other sites; and (ii) phosphorylation at T115 was inhibited by phosphorylation at S116 or the other sites. (F) Western blotting of endogenous Otx2 (left) and exogenous Otx2FL (right) with anti-Otx2 antibodies. Lysates were treated with or without λ-PP. Apparent molecular masses (kDa) of the nascent and upper-most modified bands are indicated on the right (B,D-F). Calculated and apparent molecular masses of constructs (kDa): Myc-Otx2FL, 43 and 50; Myc-Otx2ΔAD, 32 and 40; Otx2FL, 31 and 33. White arrowhead indicates a band resistant to λ-PP or incomplete digests. 3A, alanine mutant at S116, S132 and S158; 4A, alanine mutant at T115, S116, S132 and S158; blue arrowheads indicate nascent proteins; magenta arrowheads indicate modified proteins. The amount of injected mRNA (pg/embryo) was *Myc-Otx2FL* and *Myc-Otx2ΔAD*, 500; *Otx2FL*, 250. Antibodies used for western blotting (WB) or IP were as indicated.

Otx2. We first observed that western blot bands of Otx2 were not affected by either MAPKK (Kosako et al., 1993) or a MAPKK inhibitor (Fig. S4A,B). We then tried to hyperactivate endogenous Cdk activity in *Xenopus* embryos by overexpressing stable mutants of cyclin B1 (cyclin B1* for Cdk1) and cyclin A1 (cyclin A1* for Cdk1 and Cdk2), both of which lack the destruction box (Geley et al., 2001; Yamano et al., 2004). Hyperactivation of Cdks by mRNA injection of HA-cyclin B1* or HA-cyclin A1* was verified by cell-cycle arrest of mRNA-injected blastomeres (Fig. 2A, white asterisks). Under these conditions, modifications of Myc-Otx2ΔAD were dramatically enhanced (Fig. 2B,C), and these modified bands were almost removed by λ-PP treatment (Fig. 2B,C). These data suggest that Cdk is involved in the phosphorylation of Otx2.

If Otx2 is phosphorylated by cyclin/Cdks, then the S116, S132 and S158 sites might prefer either cyclin B/Cdk or cyclin A/Cdks. The data suggest that S116 and S132 preferred both cyclin B/Cdk and cyclin A/Cdks, whereas S158 preferred cyclin A/Cdks more than cyclin B/Cdk (Fig. S5), implying that cyclin B/Cdk and cyclin A/Cdks are differentially involved in the phosphorylation of Otx2.

To further examine Cdk-dependent phosphorylation of Otx2, we overexpressed the Cdk inhibitor p27xic1 in *Xenopus* embryos

Development (2018) 145, dev159640. doi:10.1242/dev.159640

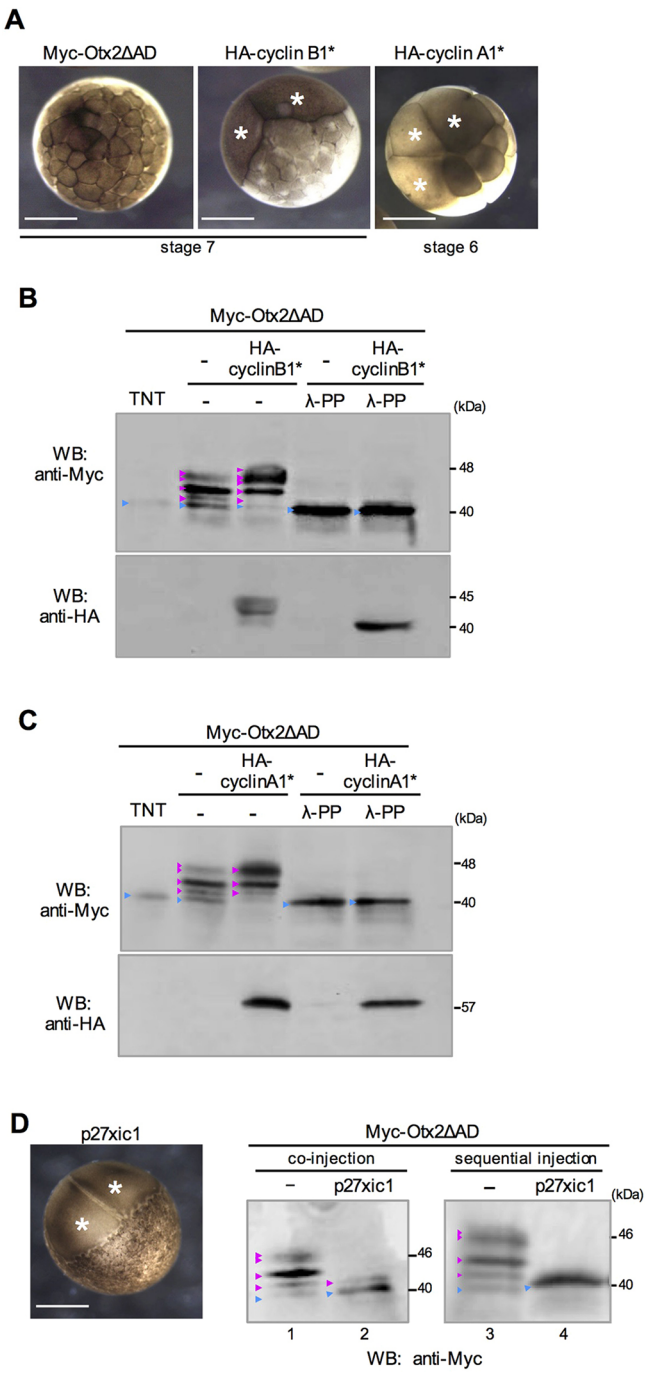

Fig. 2. Cdk-dependent phosphorylation of Otx2. (A) Cleavage arrest by HA-cyclin B1* or HA-cyclin A1*. mRNA was injected into one blastomere at the two-cell stage, and embryos were observed at the 32-cell (stage 6) or early blastula (stage 7) stage. Animal view. (B,C) Western blotting of Myc-Otx2ΔAD co-expressed with HA-cyclin B1* (B) or HA-cyclin A1* (C). Lysates were treated with λ-PP as indicated. (D) Phenotype of p27xic1-overexpressing embryos (left) and western blotting of Myc-Otx2ΔAD co-expressed with p27xic1 (middle, right). Co-injection (middle): *Myc-Otx2ΔAD* mRNA (500 pg/embryo) was co-injected with (lane 2) or without (lane 1) *p27xic1* mRNA (2 ng/embryo) into one blastomere at the two-cell stage. Sequential injection (right): *p27xic1* mRNA (1.5 ng/embryo) was injected into one blastomere at the two-cell stage, then mRNAs for *Myc-Otx2ΔAD* (500 pg/embryo) and *p27xic1* (500 pg/embryo) were co-injected into the cleavage-arrested blastomeres at the 32-cell-stage equivalent (lane 4). *Myc-Otx2ΔAD* mRNA was injected at the two-cell stage as control (lane 3). Lysates were prepared from embryos at stage 8 (B), stage 9 (C and D, lanes 1 and 2) or stage 9.5 (D, lanes 3 and 4). White asterisks indicate cleavage-arrested blastomeres. Scale bars: 500 µm in A and D.

(Vernon, 2003). We first verified cleavage arrest by *p27xic1* mRNA injection (Fig. 2D, left, white asterisks) as reported elsewhere (Ohnuma et al., 1999). When a mixture of *p27xic1* and *Myc-Otx2ΔAD* mRNAs were injected at the two-cell stage, modified bands of Myc-Otx2ΔAD were reduced, but a weak band remained, which might result from phosphorylation occurring prior to the accumulation of p27xic1 protein translated from the injected mRNA (Fig. 2D, lanes 1, 2). Therefore, we first injected *p27xic1* mRNA alone at the two-cell stage, followed by injection of Myc-Otx2ΔAD mRNA into the cleavage-arrested blastomeres at the 32-cell-stage equivalent. p27xic1 completely abolished modified bands of Myc-Otx2ΔAD (Fig. 2D, lanes 3 and 4), suggesting that phosphorylation of Otx2 depends on Cdk activity. These data also imply that the reduction of modified Otx2 by p27xic1 expression was not caused by dephosphorylation, because, once Otx2 was phosphorylated at the 2- to 32-cell stages (lane 2), it appeared to be stable until the late blastula stage when western blotting was performed (compare lanes 2 and 4 in Fig. 2D). Given that phosphorylation of Otx2 appears to start early in development, we examined developmental changes in phosphorylation levels using Myc-Otx2ΔAD and Myc-Otx2FL (Fig. S5D,E). The data showed that modification of Otx2ΔAD was already detectable at the 16-cell stage (stage 5), gradually increased until the early gastrula stage (stage 10.5) (Fig. S5D; see boxed areas for WT), and then reached almost a plateau at stage 10.5 onwards (Fig. S5E). The increase in phosphorylation levels until stage 9 correlates well with the cleavage cycle, supporting again the possibility that Otx2 is a substrate of cyclin/Cdks.

Taken together, Otx2 has four possible phosphorylation sites, and we refer to T115 as A-site (putative Akt site) and S116, S132 and S158 as C-sites (putative Cdk sites) in the following experiments.

Otx2 mutants 4A and 4E have distinct functions in eye formation

To determine whether known Otx2 activities are affected by phosphorylation states, we overexpressed phosphomimetic or nonphosphorylatable Otx2 in *Xenopus* embryos and analyzed the resulting eye phenotypes, which have been well documented for Otx2 functions (Martinez-Morales et al., 2001; Nishihara et al., 2012). A phosphomimetic mutant, named Otx2-4E, was made by replacing A-site (T115) and three C-sites (S116, S132 and S158) with glutamate in Otx2FL. Nonphosphorylatable mutants, named Otx2-T115A, -3A and -4A, were similarly made by replacing A-site, C-sites or all four sites with alanine, respectively. Each Otx2 construct was expressed unilaterally in the anterior neuroectoderm, which includes the eye field, and the phenotypes were scored at stages 38-42. We categorized abnormal eye phenotypes into three types compared with the normal-looking phenotype (Fig. 3A-D). Expression of Otx2-WT, -4E -T115A, or -3A caused small/trace eye and ventral defect phenotypes in a dose-dependent manner (Fig. 3E), in which stronger phenotypes appeared to be obtained by expression of Otx2-WT, -4E, -3A and -T115A in order. By contrast, only Otx2-4A caused enlarged eye phenotypes, which have not previously been reported following the expression of any other Otx2 mutants in *Xenopus* (Andreazzoli et al., 1997; Isaacs et al., 1999). Notably, both Otx2-T115A and -3A reduced rather than enlarged the eyes (Fig. 3E), indicating that both mutations are necessary for the activity of Otx2-4A. Quantitative analysis of the area of the eye vesicle showed that eye size in Otx2-4A-expressing embryos was enlarged by approximately 1.3 times, whereas that in Otx2-4E-expressing embryos was reduced by approximately 0.5 times, compared with control (Fig. 3F). Section examination of the enlarged eye phenotype by Otx2-4A showed that the retinal tissue was expanded ventrally with a reduction in the retinal

Development (2018) 145, dev159640. doi:10.1242/dev.159640

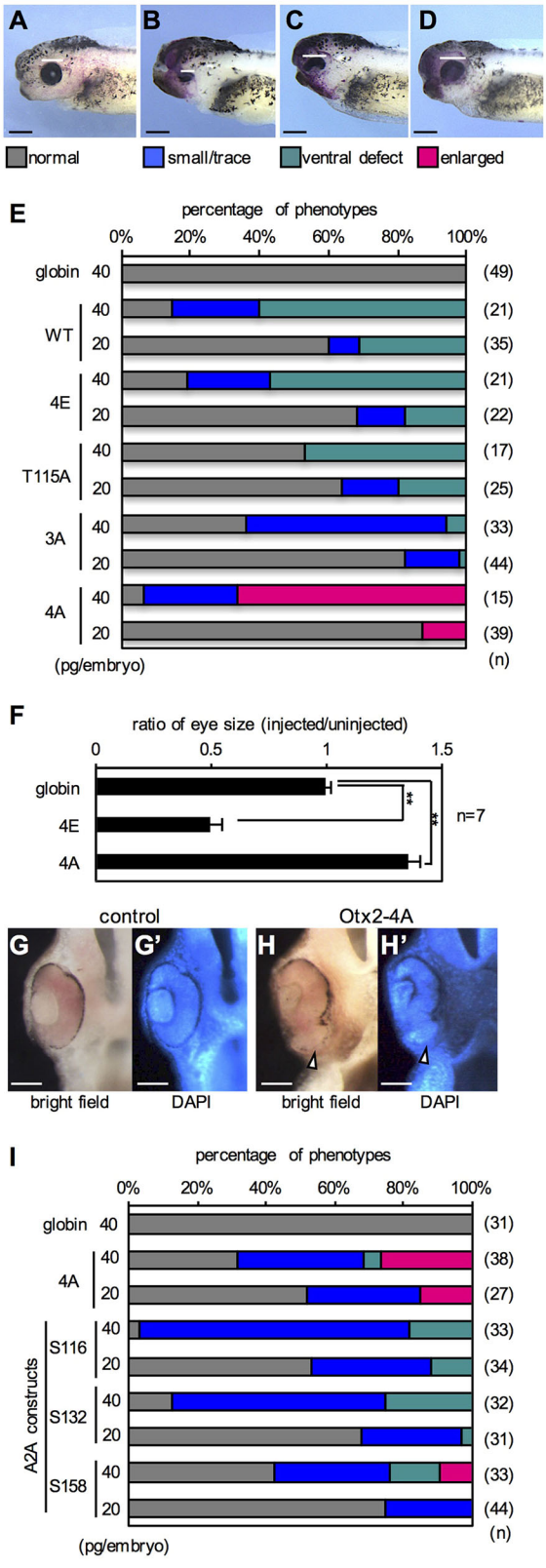

Fig. 3. Eye phenotypes caused by Otx2 mutants. (A-D) Representative eye phenotypes. mRNAs for Otx2 construct and *nbgal* as a tracer were co-injected into the presumptive eye field of the dorsal-left blastomere at the four-cell stage. Phenotypes were scored at stages 38-42: normal indicates normal-looking eyes; small/trace indicates small or trace eye; ventral defect indicates normal eye width with pigmentation defect on the ventral side; enlarged indicates enlarged eye. Some injected embryos showed gastrulation arrest, which were removed from the total scores. White bars indicate the diameter of the eye. Anterior to the left, dorsal is up. (E) Incidence of eye phenotypes. See A-D for color codes of phenotypes. mRNAs for Otx2 construct or globin (negative control) was injected at 20 or 40 pg/embryo as indicated. *n* indicates the total number of scored embryos. (F) Quantitative analysis of the eye size. $^{**}P<0.01$ (Student's *t*-test); error bars, s.e.m.; *n* indicates the number of samples. (G-H′) Transverse hemisection across the left eye. (G,G′) Control. (H,H′) Enlarged eye caused by Ox2-4A. (G,H) Bright field. (G′,H′) DAPI staining. Arrowheads indicate pigmentation defect in the ventral retina. (I) Incidence of eye phenotypes caused by Otx2-A2A constructs. In the A2A constructs, the remaining intact serine residue is indicated. Scale bars: 500 µm in A-D; 100 µm in G,H.

pigment epithelium (Fig. 3H,H′, arrowheads) compared with the control (Fig. 3G,G′). These results clearly demonstrated that Otx2-4A has different activities in eye formation compared with the other mutants, and that exogenous Otx2-WT functions in a phosphorylated form, given that WT exhibits similar activities to 4E (Fig. 3E).

To further examine whether all C-site mutations are required for the activity of Otx2-4A, we constructed triple-alanine mutants of Otx2 (named A2A constructs), in which only one of the C-sites (S116, S132 or S158) was intact, referred to as A2A-S116, -S132 or -S158, respectively. A2A-S116 and A2A-S132 both caused small/trace and ventral defect eye phenotypes (Fig. 3I). By contrast, A2A-S158 caused an enlarged eye phenotype in a dose-dependent manner, although the fraction of enlarged eye phenotypes by A2A-S158 was lower than that of Otx2-4A. These data indicate that mutations at T115, S116 and S132 are essential for enlarged eye phenotypes.

We next examined the early effect of Otx2-4A and -4E by focusing on the eye field marker gene *rax*. Overexpression of Otx2-4A increased the expression of *rax* compared with the uninjected side (Fig. 4D), whereas Otx2-WT and -4E as well as the globin control did not affect *rax* expression (Fig. 4A-C). The expansion of *rax* expression by Otx2-4A could explain the enlarged-eye phenotypes seen in these embryos. The enlarged eye phenotypes with aberrant ventral eye structures (Fig. 3H,H′) also suggested that Otx2-4A converts the presumptive optic stalk to the retina. Therefore, we examined the expression of *pax2* and *pax6* in the late neurula, in which *pax2* is expressed in the optic stalk (OS) and MHB (Fig. 4E), whereas *pax6* is expressed in the optic vesicle (OV) and diencephalon (Di) side by side with different whole-mount *in situ* hybridization (WISH) intensities (Fig. 4I). Overexpression of Otx2-WT, -4E and -4A all inhibited *pax2* expression in the OS (Fig. 4E-H), whereas Otx2-WT and -4E, but not -4A caused a posterior shift in *pax2* expression in the MHB (open arrowheads in Fig. 4E-H). The reduction in *pax2* in the OS by Otx2-WT, -4E and -4A (Fig. 4F-H) is consistent with the aberrant eye morphology at the tailbud stage on the ventral side where the OS is formed (Fig. 3C,E). Otx2-WT, -4E and -4A differently affected the expression of *pax6*. WT reduced OV but expanded Di *pax6* expression (Fig. 4J,J′; dashed black lines, Di; dashed white lines, OV); and Otx2-4E slightly reduced *pax6* OV expression similar to WT (Fig. 4K,K′), consistent with the small/trace eye phenotypes of these embryos (Fig. 3B,E). By contrast, Otx2-4A expanded OV *pax6* expression (Fig. 4L,L′), consistent with its enlarged eye phenotypes (Fig. 3D,E). These data demonstrated that Otx2-4E and -4A have different activities in eye formation. This raised the next question of whether Otx2-4E and -4A have different activities in cell proliferation and anteroposterior patterning, which have been reported for Otx2 (Pilo et al., 2001; Acampora et al., 2000).

Development (2018) 145, dev159640. doi:10.1242/dev.159640

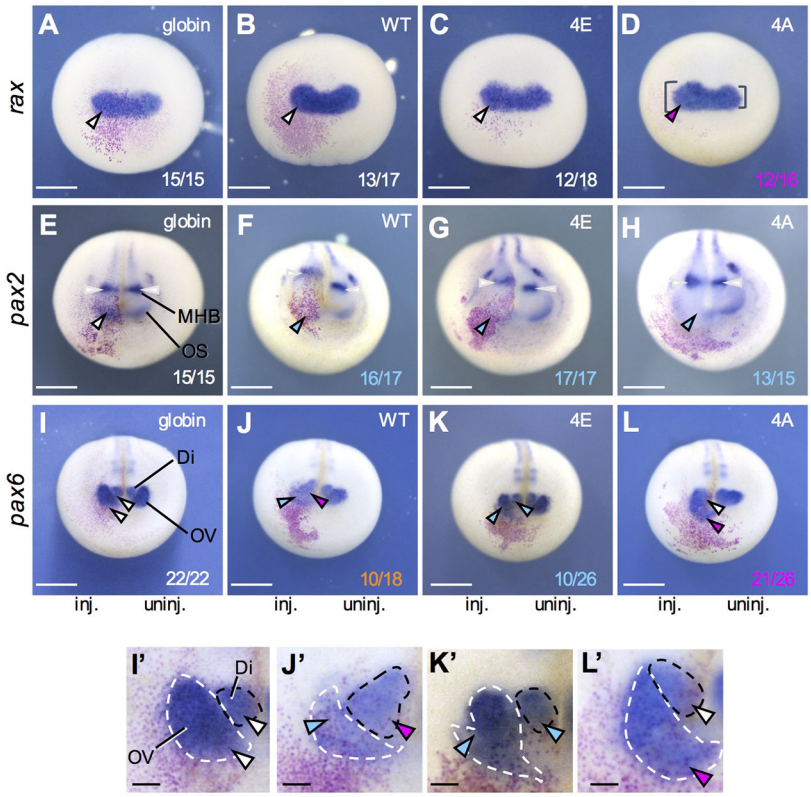

Fig. 4. Effects of Otx2 mutants on eye marker genes. Embryos were co-injected on the right side with mRNA for globin, WT, 4E or 4A (20 pg/embryo) and *nbgal* as described in the legend to Fig. 3, and were subjected to WISH for *rax* (A-D), *pax2* (E-H) and *pax6* (I-L) at early neurula stages (stages 13-14, A-D) or late neurula stages (stages 18-20, E-L). The fractions indicate the proportion of the presented phenotype per total number. Colors of numbers: white indicates normal expression; magenta indicates upregulation; blue indicates downregulation; orange indicates combined effects of enlarged Di and reduced OV. Square brackets indicate the sizes of the eye field showing the difference between left and right. Open arrowhead indicates the position of MHB. Anterior view with dorsal up. (I′-L′) Enlarged images of I-L. Dashed black and white lines indicate Di and OV, respectively, where *pax6* is expressed. Colors of arrowheads: white indicates normal expression; magenta indicates upregulation; blue indicates downregulation (A-L′). Scale bars: 500 µm in A-L; 100 µm in I′-L′.

Otx2-4E stimulates cell proliferation

To investigate the effect of Otx2 on cell proliferation, Otx2-4E or -4A was expressed in the dorsoanterior region of the embryo, and immunostaining was then performed for phospho-histone H3 (PH3) as a mitosis marker. The numbers of PH3-positive nuclei were counted in EGFP-positive and negative areas for quantitative analysis (Fig. 5A-C). The data showed that the ratio of the number of PH3-positive nuclei in injected versus uninjected areas was 1.27 ±0.07 (mean±s.e.m.) and 1.38±0.05 in Otx2-WT and -4E-expressing embryos, respectively, whereas it was 0.727±0.062 in Otx2-4A-expressing embryos. These ratios significantly differed from the control (0.944±0.014) (Fig. 5D), suggesting that Otx2-WT and -4E both stimulate cell proliferation, whereas Otx2-4A reduces it. To confirm this, we counted the number of nuclei stained by DAPI (Fig. 5E-G). Quantitative analysis showed that the ratio of cell number in injected versus uninjected areas was 1.08±0.061 and 1.13± 0.02 in Otx2-WT- and -4E-expressing embryos, respectively, whereas it was 0.894±0.019 in Otx2-4A-expressing embryos. The ratios in 4E and 4A embryos differed significantly from the control (1.02± 0.04; P<0.05) (Fig. 5H). Thus, these data suggest that Otx2-4E and -4A have opposite effects on cell proliferation: Otx2-4E stimulates whereas -4A reduces proliferation.

To examine the *in vivo* relevance of Otx2 function in cell proliferation, we next performed loss-of-function experiments using antisense morpholino oligos (MOs) for *otx2* and its functionally redundant paralog *otx5*, according to our previous report (Yasuoka et al., 2014). The number of PH3-positive nuclei was almost unchanged in the anterior neuroectoderm injected with standard control MO (Fig. S6A-A″,C), whereas it significantly decreased in the region injected with *otx2*/*otx5*-MOs (Fig. S6B-B″,C). Consistent with this, the number of nuclei decreased in the *otx2*/*otx5*-MO-injected area (Fig. S6E-E″,F), but not affected in the control MO-injected area (Fig. S6D-D″,F). These data indicate that Otx2 and Otx5 are required for cell proliferation in the anterior neuroectoderm, and these *in vivo* data are consistent with the enhancement of cell proliferation by exogenous Otx2-WT and -4E (Fig. 5). This also suggests that the reduction in cell proliferation caused by Otx2-4A results from the dominant-negative action of Otx2-4A against endogenous phosphorylated Otx2, which stimulates cell proliferation, and the unphosphorylated form of Otx2 is unable to take its place.

To determine how Otx2 stimulates proliferation, we focused on *p27xic1* because Otx2 reportedly inhibits the *p27* gene (Bunt et al., 2012). Analysis of our ChIP-seq data using the *X. tropicalis* gastrula (Yasuoka et al., 2014) showed the co-occupancy of Otx2 and Tle1 of several potential CRMs near *p27xic1* (Fig. 6A), suggesting that *p27xic1* is a direct target gene of Otx2. Using mRNA injection, Otx2-WT, -4E or -4A with nuclear β-galactosidase (n*β*-gal) as a tracer were unilaterally expressed, and the expression of *p27xic1* was examined by WISH. Expression of Otx2-WT and -4E, but not of -4A, downregulated *p27xic1*, compared with globin-injected negative control and on the uninjected side (Fig. 6B-E′), consistent with the stimulation of cell proliferation by Otx2-4E (Fig. 5D,H).

To assess the gain-of- and loss-of-function data discussed above, the expression domains of *otx2* and *p27xic1* and the distribution of PH3-positive cells in the early neurula were examined using sagittal hemisections. The data showed that the *otx2*-expressing region did not overlap with that of *p27xic1* (Fig. 6F-G′) and had more mitotic cells than the posterior region (Fig. 6H,H′), consistent with the involvement of *otx2* in cell proliferation in the anterior neuroectoderm. These data suggest the existence of a positive feedback loop involving Otx2, Cdk and p27xic in the regulation of cell proliferation (Fig. 6I).

Activities of Otx2-4E and -4A in anteroposterior patterning

In the neural plate, Otx2 is involved in anteroposterior patterning by directly inhibiting posterior genes, which are suggested to include

Development (2018) 145, dev159640. doi:10.1242/dev.159640

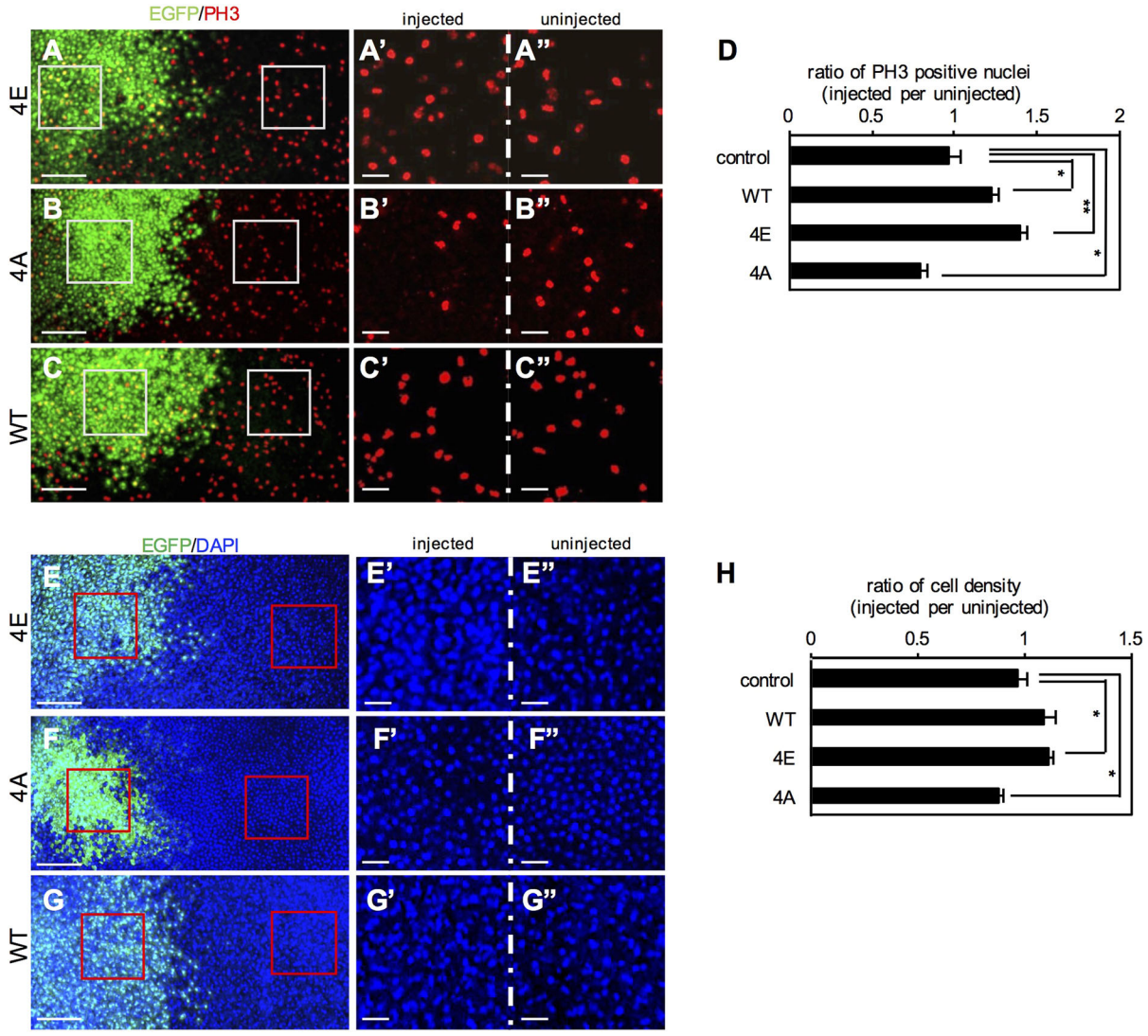

Fig. 5. Phosphomimetic Otx2-4E stimulates cell proliferation. (A-C) mRNA for Otx2-4E (A), -4A (B) or -WT (C) together with EGFP as a tracer was injected into one blastomere at the four-cell stage. Embryos were immunostained for PH3 at the late gastrula stage. PH3-positive nuclei are shown in red, Otx2 mutant-expressing cells (expressing EGFP) are shown in green. White boxes indicate enlarged areas (A′-C″). (D) Quantitative analysis of PH3-positive nuclei. More than 90 PH3-positive nuclei were counted in one embryos, and six to ten embryos were analyzed for calculating the mean ratio (and s.e.m.) of the number of PH3-positive nuclei in injected versus uninjected areas. (E-G) Representative images of DAPI-stained nuclei in Otx2-4E (E), -4A (F) or -WT (G)-expressing gastrula embryos. Nuclei are shown in blue, and Otx2 mutant-expressing cells (expressing EGFP) are shown in green. Red boxes indicate enlarged areas (E′-G″). The dorsoanterior region was observed. (H) Quantitative analysis of cell numbers. More than 500 nuclei in total were counted in one embryo, and five to seven embryos were analyzed for calculating the mean ratio (and s.e.m.) of the number of nuclei in injected versus uninjected areas. ***P*<0.01, **P*<0.05 (Student's *t*-test); error bars, s.e.m. (D,G). Scale bars: 200 µm in A-G; 50 µm in A′-G″.

gbx2 and *meis3* (Yasuoka et al., 2014), and by directly activating anterior genes, such as *xcg1* (Gammill and Sive, 1997) and *rax* (Danno et al., 2008). We first examined *gbx2* by ectopically expressing Otx2-WT, -4E or -4A, in the posterior neuroectoderm. Both Otx2-WT and -4E downregulated the expression of *gbx2* (Fig. 7B-C′, arrowheads) compared with the uninjected side and globin-injected control (Fig. 7A,A′). This activity explains the posterior shift in *pax2* expression in the MHB by Otx2-WT and -4E (Fig. 4F,G). Conversely, Otx2-4A did not downregulate *gbx2* expression (Fig. 7D,D′), suggesting that only phosphorylated Otx2 has the ability to inhibit posteriorization.

xcg1 is expressed in the cement gland, which is the anterior-most organ (Fig. 7E). Ectopic expression of Otx2-WT, -4E and -4A all upregulated *xcg1* (Fig. 7F-H), and this activation was observed in the ventrolateral ectoderm, but not in the neuroectoderm, as reported elsewhere (Gammill and Sive, 1997). To assess whether the ectopic upregulation of *xcg1* by the Otx2 mutants required their transactivation activity, we developed transactivation domain-deleted constructs of 4E (ΔAD-4E) and 4A (ΔAD-4A). Neither ΔAD-4E- nor ΔAD-4A upregulated *xcg1* (Fig. 7I,J), indicating that the transactivation domain of Otx2-4E and -4A is required for their activation of *xcg1*. These data also suggest that Otx2 has transactivation activity regardless of its phosphorylation state.

The above data suggest that the difference in function between Otx2-4E and -4A is repression activity. To further examine whether phosphorylation states affect the repression and activation activity of Otx2, we performed luciferase reporter assays. We first examined the response of the silencer of *meis3*, a posterior gene, which is expected to be repressed by Otx2. The *meis3*-D2 silencer (Yasuoka et al., 2014) was inserted upstream of the SV40 promoter in the

Development (2018) 145, dev159640. doi:10.1242/dev.159640

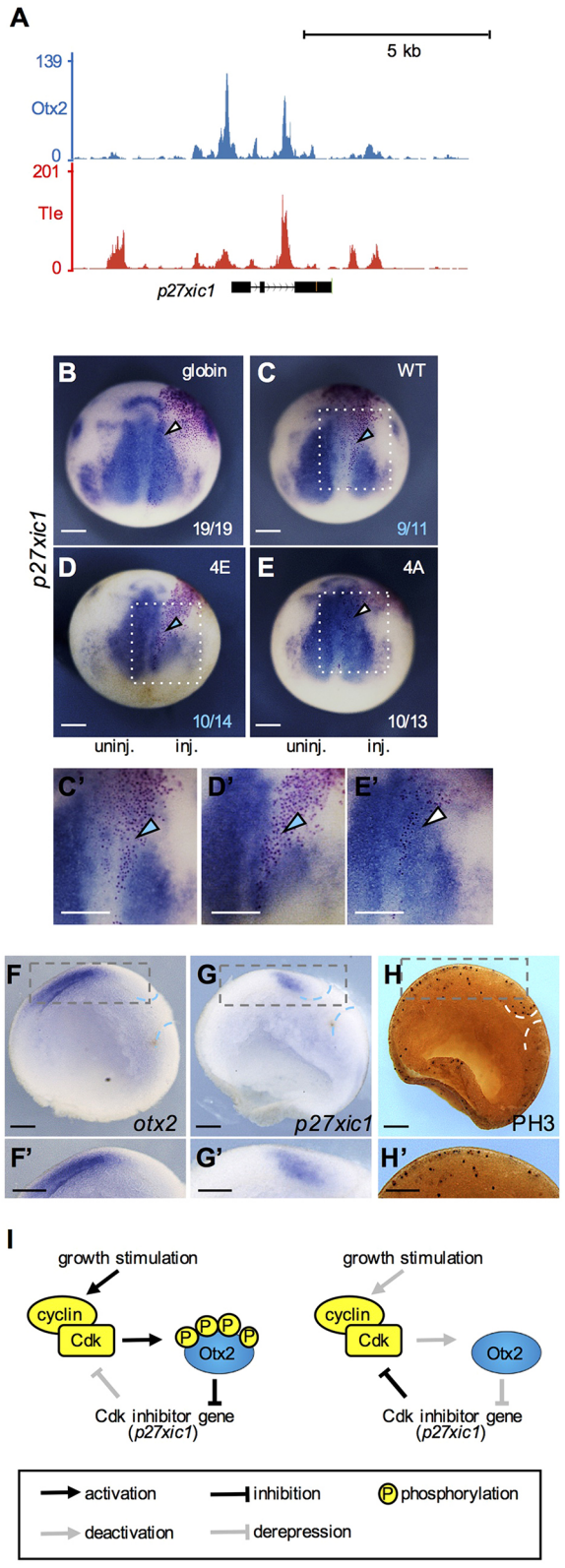

Fig. 6. Phosphomimetic Otx2-4E negatively regulates *p27xic1*. (A) Genome browser representation showing occupancies of Otx2 and Tle in *Xenopus tropicalis* gastrula embryos around the *p27xic1* gene. (B-E) WISH analysis of *p27xic1* at the neurula stage (stages 13-14). mRNA (30 pg/embryo) for globin (B), WT (C), 4E (D) or 4A (E) together with *nbgal* mRNA was injected in the presumptive posterior neuroectoderm at the four-cell stage. Dorsal view with anterior up. inj. indicates the injected side; uninj. indicates the uninjected side. Colors of numbers and arrowheads are the same as in Fig. 4. (C′,D′,E′) Enlarged image of C, D and E (dotted white box). (F-H) WISH and immunostaining of sagittal hemisection. WISH for *otx2* and *p27xic1* (F,G). Immunostaining of PH3 (H). Dorsal up, anterior to the left. (F′,G′,H′) Enlarged images of F,G, H (dashed gray box). Dashed blue or white lines indicate the position of the blastopore. (I) A schematic model of feedback loops involving Cdk, Otx2 and p27xic in cell-proliferation (left) and non-proliferation states (right). Left, upon growth stimulation, (1) activation of Cdk causes phosphorylation of Otx2; (2) phosphorylated Otx2 downregulates *p27xic1*; and (3) the reduction in p27xic1 increases Cdk activity, thereby enhancing both cell proliferation and a phosphorylation state of Otx2. Right, upon the reduction of growth stimulation, (1) reduced Cdk activity causes the reduction of phosphorylation of Otx2; (2) the reduction in phosphorylated Otx2 derepresses *p27xic1*; and (3) increased p27xic1 inhibits Cdk activity, thereby reducing both cell proliferation and a phosphorylation state of Otx2. Scale bars: 300 µm in B-H,C′-H′.

reporter construct, and this reporter alone showed a high level of luciferase activity in the animal pole region. Under this condition, reporter activity was significantly repressed by Otx2-WT and -4E, but not by -4A (Fig. 7K). We next tested the combinatorial repressive activity of Otx2 with the interacting partner Gsc and the co-repressor Tle1, which form the repression complex for negative target genes of Otx2 (Yasuoka et al., 2014). Repression of the *meis3-D2* reporter by Gsc and Tle1 was enhanced by co-expression of Otx2-WT, and this enhancement was also observed with Otx2-4A (Fig. 7L), suggesting that phosphorylation of Otx2 is not required for, and neither does unphosphorylated Otx2 interfere with, the formation of a ternary repression complex. Given that Otx2-4A and Tle1 did not repress the reporter (Fig. 7L), repression activity by a combination of Otx2-4A, Gsc and Tle1 probably results from recruitment of Tle1 to Gsc. Although Otx2-4A does not interfere with complex formation, Otx2-4A might weaken the repression activity of the complex, as implied in Fig. S7 (compare Otx2-4A with Otx2-4E).

We next examined an activated target gene of Otx2, *rax*, using the reporter gene SOP-FLASH, which has eight tandemly repeated *rax* enhancer elements binding for Otx2 and Sox2 (Danno et al., 2008). The data showed that both Otx2-4E and -4A exerted transactivation activity (Fig. 7M), similarly to activation of the *xcg1* gene by Otx2-4E and -4A (Fig. 7G,H). Given that Sox2 is expressed in the neuroectoderm (Mizuseki et al., 1998) and has a transactivation domain (Nowling et al., 2000), a combination of Sox2 and Otx2 could function as an activator regardless of the phosphorylation states of Otx2. In addition, because Otx2-4E did not upregulate the endogenous *rax* gene (Fig. 4C), activation of the *rax* reporter by Otx2-4E might result from the CRM boosted by eight tandem repeats. Taken together, it is suggested that phosphorylation of Otx2 is required for its repression activity but does not affect the transactivation activity of this protein.

Otx2-4E, but not -4A interacts with Tle1

The eh1 repression domain of Otx2 reportedly interacts with TLE/Groucho (Heimbucher et al., 2007). Therefore, we tested the physical interaction between Otx2 mutants and HA-tagged Tle1 by co-immunoprecipitation (Co-IP) assays (Fig. 7N). A co-immunoprecipitated band of HA-Tle1 was detected with Myc-Otx2-4E as well as with Myc-Otx2-WT (magenta arrowheads in Fig. 7N), but barely with Myc-Otx2-4A, consistent with the data that neither Otx2-4A alone nor co-expression with Tle1 exerted repressive activity on the *meis3-D2* luciferase reporter (Fig. 7K,L). The reason why the intensity of the co-immunoprecipitated Tle1 band with WT was weaker than that of 4E (Fig. 7N) might be because of the partial phosphorylation of WT. These data suggest that phosphorylation of Otx2 is required for the interaction with

Development (2018) 145, dev159640. doi:10.1242/dev.159640

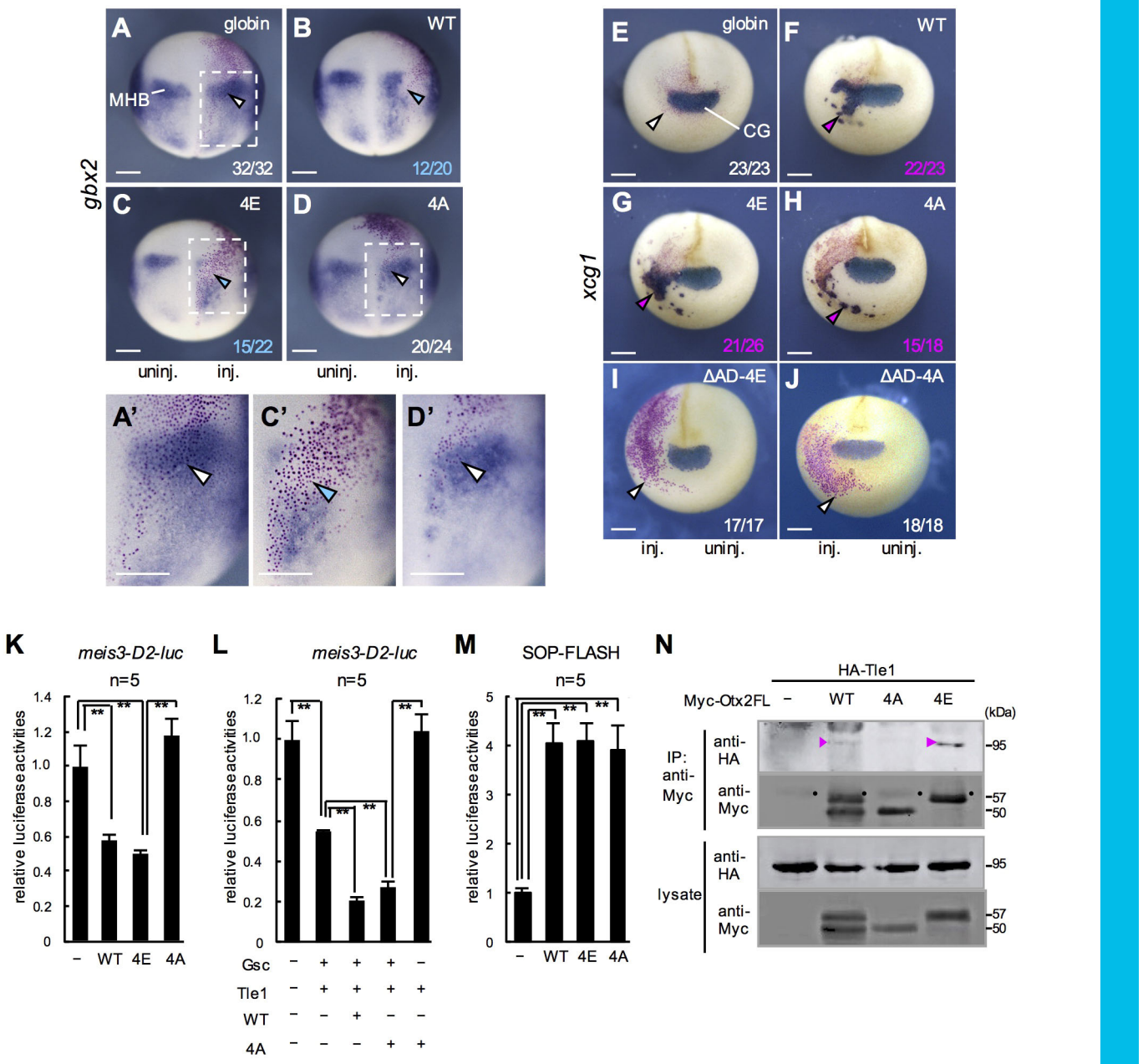

Fig. 7. Repression and/or activation activities of Otx2-4E and -4A and Tle interaction. (A-D) WISH for *gbx2* at the late gastrula to early neurula stage (stages 12.5-13). Dorsal view with anterior up. (A′,C′,D′) Enlarged images of A, C and D (dashed white box). (E-J) WISH for *xcg1* at the late neurula stage (stages 18-20). Anterior view with dorsal up. CG indicates the cement gland. mRNA injection was the same as in Fig. 6. Colors of numbers and arrowheads are the same as in Fig. 4. (K-M) Luciferase reporter assays. *meis3*-D2-luc reporter DNA was co-injected with mRNA for Otx2-WT, -4E or -4A (50 pg/embryo) (K) or with combinations of mRNAs for Gsc (12.5 pg/embryo), Tle1 (12.5 pg/embryo), Otx2-WT and -4A (25 pg/embryo) as indicated (L). SOP-FLASH reporter DNA was co-injected with mRNA for Otx2-WT, -4E or -4A (50 pg/embryo) (M). ***P*<0.01 (Student's *t*-test); error bars, s.e.m.; N.S., not significant; *n* indicates the number of samples. (N) Physical interaction between Tle1 and Otx2FL mutants as assayed by Co-IP. The amounts of expressed protein were verified by western blotting (lower panels). Apparent molecular masses (kDa) of Myc-Otx2FL-WT, -4A and -4E were 50, 50 and 57, respectively. Magenta arrowheads indicate co-immunoprecipitated bands; circles indicate heavy chains of IgG from the anti-Myc antibody. Scale bars: 300 µm in A-J,A′,C′,D′.

Tle1, which enables Otx2 to then exert its own repression activity. The phosphorylation-dependent interaction of eh1 domains with TLE has not previously been reported.

DISCUSSION

Repressor activity of Otx2 conferred by post-translational modification

In this study, we showed that Otx2 exists in two distinct states: phosphorylated and unphosphorylated. Our data suggest that phosphorylated Otx2 functions as both a repressor and activator, whereas unphosphorylated Otx2 functions only as an activator. To date, only a few TFs have been reported to be converted from being an activator and a repressor by post-translational modification. The SoxE group of TFs, including Sox9, are converted by SUMOylation from an activator to a repressor by displacing CBP/p300 and recruiting Tle4/Grg4 (Lee et al., 2012). Another case is Pax2, transactivation of which is enhanced through JNK kinase-mediated phosphorylation in the activation domain by blocking TLE/

Development (2018) 145, dev159640. doi:10.1242/dev.159640

Groucho (Cai et al., 2003). Thus, we have shown a third case, in which phosphorylation of Otx2 enables it to function as a repressor through its interaction with Tle1 (Fig. 7N), opposite to the case of Pax2.

Otx2 has a novel eh1 domain with a Cdk site (SIWSPASISP; underlined is the possible Cdk site), which is only present in the Otx family proteins (Otx1, Otx2 and Otx5/Crx) as well as a few other TFs (Copley, 2005). The eh1 domain is present in many metazoan TFs (Copley, 2005) and interacts with TLE family proteins through its conserved C-terminal WD40 repeat domain (Heimbucher et al., 2007; Pickles et al., 2002). Given that some WD40 domains of ubiquitin ligases and phosphatases, such as β-Trcp and Cdc4, interact with a phosphorylated serine residue in their substrates (Yaffe and Elia, 2001), it is possible that one of the WD40 repeats of TLE interacts with the eh1 domain with a phosphorylated site in Otx2.

Role of cyclin/Cdk-dependent phosphorylation of TFs

We propose a positive feedback loop model for Otx2 functions in cell proliferation (Fig. 6I). In this model, in a proliferative state, Otx2 is phosphorylated to repress target genes, including *p27xic1* as well as *gbx2* and *meis3*, whereas, when the cell cycle is arrested, unphosphorylated Otx2 increases to activate the target genes, *rax* and *pax6*. Thus, the phosphorylated and unphosphorylated states of Otx2 can be toggled by the cell cycle. However, it is not known how the phosphorylated state of Otx2 is changed to the unphosphorylated state. There are two possibilities: (1) dephosphorylation of Otx2 by phosphatase; and (2) degradation of phosphorylated Otx2. We did not observe any differences in the instability of the Otx2-4E mutant compared with -4A by western blotting (not shown), which does not support the second possibility, and denies phosphorylation-dependent degradation. A putative PEST sequence, an indicator of rapidly degraded protein, is present in the *Xenopus* Otx2 protein (Mori et al., 1994; Williams and Holland, 1998), and Otx2 might have a short half-life. Therefore, unphosphorylated Otx2 could be generated through the rapid turnover of Otx2 regardless of its phosphorylation state.

We showed that endogenous Otx2 is phosphorylated, but that its phosphorylation levels were lower than those of exogenous Otx2 (Fig. 1F). This difference might be caused by the timing of protein production and the number of proliferating cells where phosphorylation of Otx2 supposedly occurs. For exogenous Otx2, mRNA was injected into the animal pole region at two- or four-cell stages, and translated in the presumptive ectoderm from early cleavage stages; the translation product was phosphorylated until the blastula stage (Fig. S5D,E) by Cdk1 activity, which oscillates with a period of ∼30 min during the cleavage cycle (Hörmanseder et al., 2013). By contrast, in the *in vivo* situation, the transcription of *otx2* starts in the dorsal endoderm and mesoderm at the late blastula stage and in the dorsal ectoderm at the early gastrula stage (Sudou et al., 2012); endogenous Otx2 protein then accumulates in the head organizer and the anterior neuroectoderm, and the proliferation rates in these regions dramatically decrease, especially in the head organizer (Fig. 6H). Therefore, even if phosphorylation levels of endogenous Otx2 in proliferating cells are high, the average phosphorylation level of Otx2 in major nonproliferating and minor proliferating cell populations in a gastrula or neurula embryo is lower than those of exogenous Otx2.

We have proposed a positive feedback loop involving Cdk-dependent phosphorylation of Otx2 for cell proliferation (Fig. 6I). Similar feedback loops involving other TFs are also reported, but the regulatory mode is different from that of Otx2. That is, TFs are switched 'on' or 'off' by Cdk-dependent phosphorylation to promote cell cycle progression. An example of regulation by an 'on' switch is Foxm1. Foxm1 is activated by the phosphorylation of the N-terminal inhibitory domain by cyclin/Cdk to upregulate cyclin B and cdc25B, thereby forming a positive feedback loop for cell proliferation (Park et al., 2008; Major et al., 2004). An example for an 'off' switch is Foxo. Foxo upregulates the Cdk inhibitor genes *p27kip1* and *p21WAF1*, but, upon phosphorylation by cyclin/Cdk, undergoes nuclear export, which almost switches off the function of Foxo, leading to cell proliferation (Schuff et al., 2010; Liu et al., 2008; Stahl et al., 2002). In the case of Otx2, Cdk-dependent phosphorylation confers repressor activity to Otx2 for repressing *p27xic*; otherwise, it functions as an activator on its own, as mentioned above, which differs from simple switch 'on' or 'off' regulation.

Regarding tissue specification and differentiation, Cdk-dependent phosphorylation generally negatively regulates the activity of TFs that directly activate differentiation genes. For example, the phosphorylation of the myogenic TF MyoD by cyclin/Cdk leads to its degradation to prevent muscle differentiation (Kitzmann et al., 1999). During neurogenesis, the Cdk-dependent phosphorylation of neurogenin 2 (Ngn2, or Neurog2) inhibits its neural differentiation activity (Ali et al., 2011; Hindley et al., 2012). In these cases, Cdk-dependent phosphorylation of the TFs switches off their functions. Taken together, phosphorylation of TFs by cyclin/Cdks either promotes cell cycle progression (e.g. Foxm1 and Foxo) or inhibits tissue differentiation (e.g. MyoD and Ngn2). By contrast, Cdk-dependent phosphorylation not only inhibits the function of Otx2 in differentiation, but also converts it to be able to function in proliferation. Thus, this study has revealed a new category of TFs, in which post-translational modification of a single TF converts it from having a differentiation- to a proliferation-orientated role.

How does Otx2 coordinate its activator and repressor functions?

How Otx2 properly functions as an activator or a repressor for its target genes, and coordinates proliferation, tissue patterning and differentiation during embryogenesis, has been unclear. One answer to this question was reported in our previous paper (Yasuoka et al., 2014), showing the combinatorial regulation of target genes with Lim1 (activator) or Gsc (repressor). In the current study, we showed the post-translational regulation of Otx2 activity to be another answer, in which phosphorylation of Otx2 confers repressor activity at least partly through its interaction with Tle1. However, how the combinatorial and post-translational regulations work together remains elusive.

During eye formation, it was reported that expression of a repressor form of Otx2 (Otx2-EnR) by mRNA injection in *Xenopus* embryos results in a small eye or eyeless phenotype (Isaacs et al., 1999), and that expression of another type of repressor form, EnR-Otx2, in chick eyes by electroporation caused pigmentation defects of the retinal pigment epithelium and a reduction of *pax6* (Nishihara et al., 2012). These activities of repressor forms of Otx2 are similar to that of Otx2-4E in *Xenopus* embryos (Fig. 3E, Fig. 4J,K), consistent with the repressor activity of Otx2-4E (Fig. 7). In contrast with Otx2-4E, Otx2-4A expanded the expression of *rax* at early neurula stages (Fig. 4D) without stimulating cell proliferation (Fig. 5D,H); at later stages, Otx2-4A expanded the expression of *pax6* (retina) but inhibited *pax2* (OS) on the ventral side, leading to ventral expansion of the retina. These data suggest that Otx2-4A

Development (2018) 145, dev159640. doi:10.1242/dev.159640

expands the eye field, and subsequently alters patterning of the neural retina and OS. In other words, enlarged eye phenotypes caused by Otx2-4A result from changes in patterning, not proliferation. Our data are reminiscent of a previous report on the function of Otx2 for *Xenopus* retina formation, in which an activator type of Otx2 (Otx2-VP16) promotes the bipolar cell fate without stimulating retinal proliferation (Viczian et al., 2003), supporting the possibility that unphosphorylated Otx2 acts mainly as an activator in retina formation.

Several heterozygous *OTX2* mutations in human were reportedly linked with severe ocular malformation. For example, point mutations of P133T, P134A and P134R, which occur near one of the four putative phosphorylation sites, S132, found in our study (Fig. S2), are associated with microphthalmia, anophthalmia, sclerocornea and retinal detachment (Beby and Lamonerie, 2013). It is not certain whether these mutations affect the phosphorylation of Otx2 or the interaction with putative binding partners of Otx2, but it is possible that ocular defects in humans are caused by the alteration of phosphorylation states of Otx2.

In summary, we demonstrated that Otx2 undergoes phosphorylation *in vivo*, and that phosphomimetic and nonphosphorylatable mutants of Otx2 exhibit distinct activities in cell proliferation, patterning and differentiation in *Xenopus* embryos. Post-translational regulation of Otx2 repressor activity (shown here) in addition to combinatorial regulations with partner TFs (Yasuoka et al., 2014) could enable Otx2 to have versatile roles during development. *In vivo* analysis of the phosphorylation sites, such as a mutated gene knock-in approach, is now awaited to explore the role of phosphorylated Otx2 in embryonic development.

MATERIALS AND METHODS

cDNA cloning and plasmid constructs

Point mutants and deletion constructs of Otx2 were made by using PCR methods. PCR fragments of Otx2 mutants were cloned into the pCSf107mT (Mii and Taira, 2009), pCSf107_MTmT (for Myc tagging) and pCSf107_4HAmT (for HA tagging) vectors (Shibano et al., 2015), which contain SP6 terminator sequences. pGEX-GST-ΔN106cyclin B1 (Iwabuchi et al., 2002) was recloned into pCSf107_HAmT. pGEM-Δcyclin A (deletion of 55 amino acids from the N terminus of the protein) was gifted by Dr N. Furuno (Hiroshima University) before publication, and recloned into pCSf107_HAmT. All constructs made in this study are listed in Table S1.

Xenopus embryo and microinjection

Xenopus laevis and *X. tropicalis* embryos were obtained by artificial fertilization, dejellied, incubated in 0.1×Steinberg's solution (Peng, 1991), and staged according to Nieuwkoop and Faber (1967). Microinjection experiments were conducted as previously described (Yasuoka et al., 2014). For mRNA synthesis, pCSf107mT constructs with 4×SP6 terminators were transcribed with SP6 polymerase (mMESSAGE mMACHINE SP6 kit, Ambion). mRNAs were injected into one blastomere at the two- or four-cell stage. Nuclear β-galactosidase (*nbgal*) mRNA (50-100 pg/embryo) or *EGFP* mRNA (250 pg/embryo) was co-injected for lineage tracing. Antisense or standard control morpholino oligos (MOs) (Gene Tools) were injected into a dorsal blastomere at the four-cell stage. FITC-dextran (5 ng/embryo) was co-injected for lineage tracing. Sequences and specificities of antisense MOs for *X. tropicalis otx2* and *otx5* were as described previously (Yasuoka et al., 2014).

Western blotting and protein phosphatase treatment

Lysates were prepared from embryos (stages 10-10.5 unless mentioned otherwise) that had been injected with mRNA (500 pg/embryo) into both of blastomeres in the animal pole region at the two-cell stage. *In vitro* translation was performed using the TNT SP6 Quick-Coupled Transcription/Translation System (Promega) as previously described (Yamamoto et al., 2003). λ-PP treatment of lysates was carried out as previously described (Shibano et al., 2015). SDS-PAGE was carried out with 12-12.5% polyacrylamide gels. Western blotting was performed essentially as described elsewhere (Shibata et al., 2005), using anti-Myc (9E10), anti-Otx2 (Sudou et al., 2012), anti-p44/42 MAP kinase and anti-phospho-p44/42 MAPK (CST) and anti-HA (12CA5) antibodies. Apparent molecular masses (kDa) of bands were estimated based on the standard curve of size markers (BioDynamics Laboratory).

IP assays for putative phosphorylated Akt sites and the detection of endogenous Otx2 protein

Possible Akt sites of Otx2 were searched for using the database PhosphoSitePlus, (www.phosphosite.org/). IP-western assays were performed essentially as described elsewhere (Shibano et al., 2015). Immunoprecipitates with anti-Myc antibody were boiled in 2×SDS sample buffer and analyzed by western blotting with anti-Phospho-Akt Substrate antibody (CST). To detect the endogenous Otx2, we modified the preparation of the embryonic lysates. *Xenopus* neurula embryos were homogenized with lysis buffer A (50 mM Tris-Cl, pH 8.0, 10% glycerol, 0.1%NP-40, 40 µg/ml aprotinin, 20 µg/ml leupeptin, 1 mM PMSF) plus 400 mM NaCl, and homogenates were centrifuged at 4°C for 1 h at 13,200 rpm (16,000 ***g***). Supernatants were diluted four times with buffer A and centrifuged at 4°C for 1 h at 13,200 rpm. Equivalent amounts of lysate were incubated with the anti-Otx2 antibody (Sudou et al., 2012) and 25 µl protein A-agarose beads (Roche). The following wash steps of beads for IP-western assays were performed essentially as described elsewhere (Shibano et al., 2015). Immunoprecipitates with anti-Otx2 antibody were boiled in 2×SDS sample buffer and analyzed by SDS-PAGE with a 15% polyacrylamide gel and western blotting with anti-Otx2 antibody (Abcam, ab21990).

Quantitation of the eye size in tailbud-stage embryos

Embryos injected for phenotypic analysis were reared until stages 38-42 and fixed with MEMFA for 1 h. Experiments were carried out with at least three clutches. The lengths of semi-major and semi-minor axes of the eye vesicle were measured, and the eye size were calculated by using the formula for the area of an ellipse.

Immunostaining and whole-mount *in situ* hybridization

Immunostaining with anti-phospho-Histone H3 (Ser10) antibody (anti-PH3, 06-570, Merck), DAPI staining of nuclei, and counting of PH3-positive and DAPI-stained nuclei were performed as described elsewhere (Shibano et al., 2015). mRNA or MO with EGFP mRNA or FITC dextran, respectively, as a lineage tracer was injected into one blastomere at the four-cell stage. Embryos with a lineage tracer in the anterior neuroectoderm were selected for counting PH3- or DAPI-positive nuclei in an area (0.44 mm^2) in the anterior neuroectoderm on the injected or uninjected side. The effect was scored by dividing the number of nuclei on the injected side with that on the uninjected side. The statistical significance (*P* value) was calculated using Student's *t*-test after a one-way analysis of variance (ANOVA). Experiments were carried out with either four or three clutches for the mRNA or MO injection experiments, respectively. WISH was performed according to Harland (1991) with BM Purple (Roche) as a substrate. Antisense RNA probes were transcribed from linearized plasmids as described in Table S2. Experiments for WISH were carried out with two clutches for *rax*, *pax2* and *p27xic1*, and with three clutches for *pax6, gbx2* and *xcg1*. Hemisection of fixed embryos was performed as described elsewhere (Sudou et al., 2012).

Luciferase reporter assays

Embryos were co-injected with pGL4p-*meis3*-D2-luc reporter DNA and mRNA into two animal blastomeres at the two-cell stage, or co-injected with SOP-FLASH reporter (Danno et al., 2008) and mRNA into two dorsal animal blastomeres at the four-cell stage. Five pools of three injected embryos were assayed for luciferase activity at stage 10.5 for pGL4p-*meis3*-D2-luc reporter, and at stage 12 for SOP-FLASH reporter using the luciferase assay system (Promega) according to the manufacturer's protocol and as described elsewhere (Mii and Taira, 2009). Experiments were carried out at least three times; when similar results were obtained, a representative result is presented.

Co-IP assay

mRNA for HA-Tle1 (700 pg/embryo) was co-injected with or without mRNA for Myc-Otx2-WT, Myc-Otx2-4A or Myc-Otx2-4E (500 pg/embryo) into the animal pole region of both blastomeres at the two-cell stage. Embryonic lysates were prepared at stage 10.5, and subjected to Co-IP as described elsewhere (Shibano et al., 2015). Myc-Otx2 protein was co-immunoprecipitated with anti-Myc antibody and subjected to SDS-PAGE with a 10% polyacrylamide gel, followed by western blotting with anti-HA and anti-Myc antibodies.

Acknowledgments

We thank Keita Ohsumi for pGEX-GST-ΔN106cyclin B1 (a stable mutant of cyclin B1), Nobuaki Furuno for pGEM-Δcyclin A (a stable mutant of cyclin A1), Yukiko Gotoh for pSP64T-MAPKK*, and Hidetoshi Saiga and Mariko Kondo for critical reading of the manuscript. Male and female frogs of *X. tropicalis* were obtained from the National Bioresource Project (Amphibian Research Center, Hiroshima University).

Competing interests

The authors declare no competing or financial interests.

Author contributions

Conceptualization: Y.S.; Methodology: Y.S.; Validation: Y.S.; Investigation: K.M., E.H., H.O., Y.Y., T.S.; Writing - original draft: Y.S., M.T.; Writing - review & editing: Y.S., Y.Y., T.S., T.T., M.T.; Visualization: Y.S.; Supervision: M.T.; Project administration: Y.S.; Funding acquisition: M.T.

Funding

This work was supported by the Japan Society for the Promotion of Science KAKENHI grant numbers 24657147 and 25251026 (M.T.) and 17KT0114 and 16K21559 (Y.Y.).

Supplementary information

Supplementary information available online at
http://dev.biologists.org/lookup/doi/10.1242/dev.159640.supplemental

References

Acampora, D., Postiglione, M. P. I. A., Avantaggiato, V., Bonito, M. D. I. and Simeone, A. (2000). The role of Otx and Otp genes in brain development. *Int. J. Dev. Biol.* **44**, 669-677.

Agoston, Z. and Schulte, D. (2009). Meis2 competes with the Groucho co-repressor Tle4 for binding to Otx2 and specifies tectal fate without induction of a secondary midbrain-hindbrain boundary organizer. *Development* **136**, 3311-3322.

Ali, F., Hindley, C., McDowell, G., Deibler, R., Jones, A., Kirschner, M., Guillemot, F. and Philpott, A. (2011). Cell cycle-regulated multi-site phosphorylation of Neurogenin 2 coordinates cell cycling with differentiation during neurogenesis. *Development* **138**, 4267-4277.

Andreazzoli, M., Pannese, M. and Boncinelli, E. (1997). Activating and repressing signals in head development: the role of Xotx1 and Xotx2. *Development* **124**, 1733-1743.

Andreazzoli, M., Gestri, G., Angeloni, D., Menna, E. and Barsacchi, G. (1999). Role of Xrx1 in Xenopus eye and anterior brain development. *Development* **126**, 2451-2460.

Beby, F. and Lamonerie, T. (2013). The homeobox gene Otx2 in development and disease. *Exp. Eye Res.* **111**, 9-16.

Blitz, I. L. and Cho, K. W. (1995). Anterior neurectoderm is progressively induced during gastrulation: the role of the Xenopus homeobox gene orthodenticle. *Development* **121**, 993-1004.

Boyl, P. P., Signore, M., Acampora, D., Martinez-Barbera, J. P., Ilengo, C., Annino, A., Corte, G. and Simeone, A. (2001). Forebrain and midbrain development requires epiblast-restricted Otx2 translational control mediated by its 3′ UTR. *Development* **128**, 2989-3000.

Brzezinski, J. A. and Reh, T. A. (2015). Photoreceptor cell fate specification in vertebrates. *Development* **142**, 3263-3273.

Bunt, J., Hasselt, N. E., Zwijnenburg, D. A., Hamdi, M., Koster, J., Versteeg, R. and Kool, M. (2012). OTX2 directly activates cell cycle genes and inhibits differentiation in medulloblastoma cells. *Int. J. Cancer* **131**, E21-E32.

Cai, Y., Brophy, P. D., Levitan, I., Stifani, S. and Dressler, G. R. (2003). Groucho suppresses Pax2 transactivation by inhibition of JNK-mediated phosphorylation. *EMBO J.* **22**, 5522-5529.

Copley, R. R. (2005). The EH1 motif in metazoan transcription factors. *BMC Genomics* **6**, 169.

Danno, H., Michiue, T., Hitachi, K., Yukita, A., Ishiura, S. and Asashima, M. (2008). Molecular links among the causative genes for ocular malformation: Otx2 and Sox2 coregulate Rax expression. *Proc. Natl. Acad. Sci. USA* **105**, 5408-5413.

Gammill, L. S. and Sive, H. (1997). Identification of otx2 target genes and restrictions in ectodermal competence during Xenopus cement gland formation. *Development* **124**, 471-481.

Gammill, L. S. and Sive, H. (2001). otx2 expression in the ectoderm activates anterior neural determination and is required for Xenopus cement gland formation. *Dev. Biol.* **240**, 223-236.

Geley, S., Kramer, E., Gieffers, C., Gannon, J., Peters, J.-M. and Hunt, T. (2001). Anaphase-promoting complex/cyclosome-dependent proteolysis of human cyclin A starts at the beginning of mitosis and is not subject to the spindle assembly checkpoint. *J. Cell Biol.* **153**, 137-148.

Harland, R. M. (1991). Appendix G: in situ hybridization: an improved whole-mount method for Xenopus embryos. *Methods Cell Biol.* **36**, 685-695.

Heimbucher, T., Murko, C., Bajoghli, B., Aghaallaei, N., Huber, A., Stebegg, R., Eberhard, D., Fink, M., Simeone, A. and Czerny, T. (2007). Gbx2 and Otx2 interact with the WD40 domain of Groucho/Tle corepressors. *Mol. Cell. Biol.* **27**, 340-351.

Hindley, C., Ali, F., McDowell, G., Cheng, K., Jones, A., Guillemot, F. and Philpott, A. (2012). Post-translational modification of Ngn2 differentially affects transcription of distinct targets to regulate the balance between progenitor maintenance and differentiation. *Development* **139**, 1718-1723.

Holland, L. Z., Carvalho, J. E., Escriva, H., Laudet, V., Schubert, M., Shimeld, S. M. and Yu, J.-K. (2013). Evolution of bilaterian central nervous systems: a single origin? *Evodevo* **4**, 27.

Hörmanseder, E., Tischer, T. and Mayer, T. U. (2013). Modulation of cell cycle control during oocyte-to-embryo transitions. *EMBO J.* **32**, 2191-2203.

Isaacs, H. V., Andreazzoli, M. and Slack, J. M. W. (1999). Anteroposterior patterning by mutual repression of orthodenticle and caudal-type transcription factors. *Evol. Dev.* **1**, 143-152.

Iwabuchi, M., Ohsumi, K., Yamamoto, T. M. and Kishimoto, T. (2002). Coordinated regulation of M phase exit and S phase entry by the Cdc2 activity level in the early embryonic cell cycle. *Dev. Biol.* **243**, 34-43.

Katahira, T., Sato, T., Sugiyama, S., Okafuji, T., Araki, I., Funahashi, J.-I. and Nakamura, H. (2000). Interaction between Otx2 and Gbx2 defines the organizing center for the optic tectum. *Mech. Dev.* **91**, 43-52.

Kitzmann, M., Vandromme, M., Schaeffer, V., Carnac, G., Labbé, J.-C., Lamb, N. and Fernandez, A. (1999). cdk1- and cdk2-mediated phosphorylation of MyoD Ser200 in growing C2 myoblasts: role in modulating MyoD half-life and myogenic activity. *Mol. Cell. Biol.* **19**, 3167-3176.

Kosako, H., Nishida, E. and Gotoh, Y. (1993). cDNA cloning of MAP kinase kinase reveals kinase cascade pathways in yeasts to vertebrates. *EMBO J.* **12**, 787-794.

Lee, P.-C., Taylor-Jaffe, K. M., Nordin, K. M., Prasad, M. S., Lander, R. M. and LaBonne, C. (2012). SUMOylated SoxE factors recruit Grg4 and function as transcriptional repressors in the neural crest. *J. Cell Biol.* **198**, 799-813.

Liu, P., Kao, T. P. and Huang, H. (2008). CDK1 promotes cell proliferation and survival via phosphorylation and inhibition of FOXO1 transcription factor. *Oncogene* **27**, 4733-4744.

Major, M. L., Lepe, R. and Costa, R. H. (2004). Forkhead box M1B transcriptional activity requires binding of Cdk-cyclin complexes for phosphorylation-dependent recruitment of p300/CBP coactivators. *Mol. Cell. Biol.* **24**, 2649-2661.

Mallamaci, A., Di Blas, E., Briata, P., Boncinelli, E. and Corte, G. (1996). OTX2 homeoprotein in the developing central nervous system and migratory cells of the olfactory area. *Mech. Dev.* **58**, 165-178.

Martinez-Morales, J. R., Signore, M., Acampora, D., Simeone, A. and Bovolenta, P. (2001). Otx genes are required for tissue specification in the developing eye. *Development* **128**, 2019-2030.

Matsuo, I., Kuratani, S., Kimura, C., Takeda, N. and Aizawa, S. (1995). Mouse Otx2 functions in the formation and patterning of rostral head. *Genes Dev.* **9**, 2646-2658.

Mii, Y. and Taira, M. (2009). Secreted Frizzled-related proteins enhance the diffusion of Wnt ligands and expand their signalling range. *Development* **136**, 4083-4088.

Mizuseki, K., Kishi, M., Matsui, M., Nakanishi, S. and Sasai, Y. (1998). Xenopus Zic-related-1 and Sox-2, two factors induced by chordin, have distinct activities in the initiation of neural induction. *Development* **125**, 579-587.

Mori, H., Miyazaki, Y., Morita, T., Nitta, H. and Mishina, M. (1994). Different spatio-temporal expressions of three otx homeoprotein transcripts during zebrafish embryogenesis. *Mol. Brain Res.* **27**, 221-231.

Nakamura, H., Katahira, T., Matsunaga, E. and Sato, T. (2005). Isthmus organizer for midbrain and hindbrain development. *Brain Res. Rev.* **49**, 120-126.

Nieuwkoop, P. D. and Faber, J. (1967). *Normal Table of Xenopus Laevis (Daudin)*. Garland Publishing.

Nishihara, D., Yajima, I., Tabata, H., Nakai, M., Tsukiji, N., Katahira, T., Takeda, K., Shibahara, S., Nakamura, H. and Yamamoto, H. (2012). Otx2 is involved in the regional specification of the developing retinal pigment epithelium by preventing the expression of Sox2 and Fgf8, factors that induce neural retina differentiation. *PLoS ONE* **7**, e48879.

Nowling, T. K., Johnson, L. R., Wiebe, M. S. and Rizzino, A. (2000). Identification of the transactivation domain of the transcription factor Sox-2 and an associated co-activator. *J. Biol. Chem.* **275**, 3810-3818.
Ohnuma, S.-I., Philpott, A., Wang, K., Holt, C. E. and Harris, W. A. (1999). p27Xic1, a Cdk inhibitor, promotes the determination of glial cells in Xenopus retina. *Cell* **99**, 499-510.
Omodei, D., Acampora, D., Mancuso, P., Prakash, N., Di Giovannantonio, L. G., Wurst, W. and Simeone, A. (2008). Anterior-posterior graded response to Otx2 controls proliferation and differentiation of dopaminergic progenitors in the ventral mesencephalon. *Development* **135**, 3459-3470.
Owens, N. D. L., Blitz, I. L., Lane, M. A., Patrushev, I., Overton, J. D., Gilchrist, M. J., Cho, K. W. Y. and Khokha, M. K. (2016). Measuring absolute RNA copy numbers at high temporal resolution reveals transcriptome kinetics in development. *Cell Rep.* **14**, 632-647.
Pannese, M., Polo, C., Andreazzoli, M., Vignali, R., Kablar, B., Barsacchi, G. and Boncinelli, E. (1995). The Xenopus homologue of Otx2 is a maternal homeobox gene that demarcates and specifies anterior body regions. *Development* **121**, 707-720.
Park, H. J., Wang, Z., Costa, R. H., Tyner, A., Lau, L. F. and Raychaudhuri, P. (2008). An N-terminal inhibitory domain modulates activity of FoxM1 during cell cycle. *Oncogene* **27**, 1696-1704.
Peng, H. B. (1991). Xenopus laevis: pratical uses in cell and molecular biology. Solutions and protocols. *Methods Cell Biol.* **36**, 657-662.
Pickles, L. M., Roe, S. M., Hemingway, E. J., Stifani, S. and Pearl, L. H. (2002). Crystal structure of the C-terminal WD40 repeat domain of the human Groucho/TLE1 transcriptional corepressor. *Structure* **10**, 751-761.
Pilo, P., Signore, M., Annino, A., Pedro, J., Barbera, M., Acampora, D. and Simeone, A. (2001). Otx genes in the development and evolution of the vertebrate brain. *Int. J. Neurosci.* **19**, 353-363.
Schuff, M., Siegel, D., Bardine, N., Oswald, F., Donow, C. and Knöchel, W. (2010). FoxO genes are dispensable during gastrulation but required for late embryogenesis in Xenopus laevis. *Dev. Biol.* **337**, 259-273.
Shibano, T., Mamada, H., Hakuno, F., Takahashi, S.-I. and Taira, M. (2015). The inner nuclear membrane protein Nemp1 is a new type of RanGTP-binding protein in eukaryotes. *PLoS ONE* **10**, 1-21.
Shibata, M., Itoh, M., Hikasa, H., Taira, S. and Taira, M. (2005). Role of crescent in convergent extension movements by modulating Wnt signaling in early Xenopus embryogenesis. *Mech. Dev.* **122**, 1322-1339.
Spitz, F. and Furlong, E. E. M. (2012). Transcription factors: from enhancer binding to developmental control. *Nat. Rev. Genet.* **13**, 613-626.
Stahl, M., Dijkers, P. F., Kops, G. J. P. L., Lens, S. M. A., Coffer, P. J., Burgering, B. M. T. and Medema, R. H. (2002). The Forkhead transcription factor FoxO regulates transcription of p27 Kip1 and Bim in response to IL-2. *J. Immunol.* **168**, 5024-5031.
Suda, Y., Kurokawa, D., Takeuchi, M., Kajikawa, E., Kuratani, S., Amemiya, C. and Aizawa, S. (2009). Evolution of Otx paralogue usages in early patterning of the vertebrate head. *Dev. Biol.* **325**, 282-295.
Sudou, N., Yamamoto, S., Ogino, H. and Taira, M. (2012). Dynamic in vivo binding of transcription factors to cis-regulatory modules of cer and gsc in the stepwise formation of the Spemann-Mangold organizer. *Development* **139**, 1651-1661.
Vernay, B., Koch, M., Vaccarino, F., Briscoe, J., Simeone, A., Kageyama, R. and Ang, S.-L. (2005). Otx2 regulates subtype specification and neurogenesis in the midbrain. *J. Neurosci.* **25**, 4856-4867.
Vernon, A. E. (2003). A single cdk inhibitor, p27Xic1, functions beyond cell cycle regulation to promote muscle differentiation in Xenopus. *Development* **130**, 71-83.
Viczian, A. S., Vignali, R., Zuber, M. E., Barsacchi, G. and Harris, W. A. (2003). XOtx5b and XOtx2 regulate photoreceptor and bipolar fates in the Xenopus retina. *Development* **130**, 1281-1294.
Williams, N. A. and Holland, P. W. H. (1998). Gene and domain duplication in the chordate Otx gene family: insights from amphioxus Otx. *Mol. Biol. Evol.* **15**, 600-607.
Wortham, M., Jin, G., Sun, J. L., Bigner, D. D., He, Y. and Yan, H. (2012). Aberrant Otx2 expression enhances migration and induces ectopic proliferation of hindbrain neuronal progenitor cells. *PLoS ONE* **7**, e36211.
Yaffe, M. B. and Elia, A. E. H. (2001). Phosphoserine/threonine-binding domains. *Curr. Opin. Cell Biol.* **13**, 131-138.
Yamamoto, S., Hikasa, H., Ono, H. and Taira, M. (2003). Molecular link in the sequential induction of the Spemann organizer: direct activation of the cerberus gene by Xlim-1, Xotx2, Mix.1, and Siamois, immediately downstream from Nodal and Wnt signaling. *Dev. Biol.* **257**, 190-204.
Yamano, H., Gannon, J., Mahbubani, H. and Hunt, T. (2004). Cell cycle-regulated recognition of the destruction box of Cyclin B by the APC/C in Xenopus egg extracts. *Mol. Cell* **13**, 137-147.
Yasuoka, Y., Suzuki, Y., Takahashi, S., Someya, H., Sudou, N., Haramoto, Y., Cho, K. W., Asashima, M., Sugano, S. and Taira, M. (2014). Occupancy of tissue-specific cis-regulatory modules by Otx2 and TLE/Groucho for embryonic head specification. *Nat. Commun.* **5**, 4322.
Zuber, M. E. (2010). Eye field specification in Xenopus laevis. *Curr. Top. Dev. Biol.* 93, 29-60.

Fig. S1 (Satou et al.)

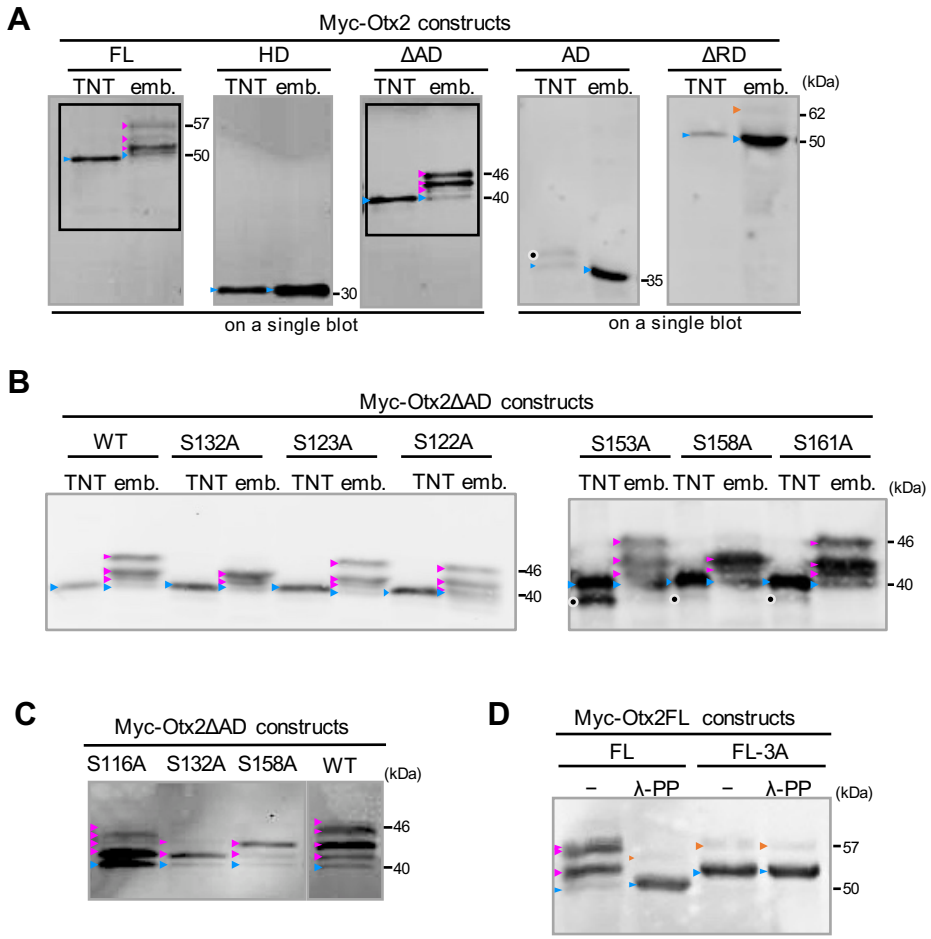

Fig. S1. Post-translational modifications of Otx2 around the repression domain. Western blot analysis of Myc-Otx2 constructs expressed in *X. laevis* embryos. (A) Myc-Otx2 (FL) and its deletion constructs (HD, ΔAD, AD and ΔRD). Boxes indicate the data presented in Fig. 1B. ΔRD appeared to have a modified band (orange arrowhead). (B) WT and alanine mutants at S132 (S132A), S123 (S123A), S122 (S122A), S153 (S153A), S158 (S158A) and S161 (S161A) in Myc-Otx2ΔAD constructs. (C) WT and alanine mutants at S116 (S116A), S132 (S132A), S158 (S158A) in Myc-Otx2ΔAD constructs. (D) λ-PP treatment removed most modified bands of WT and 3Aconstructs of Myc-Otx2FL. Note that the different electrophoretic mobility of nascent bands (blue arrowheads) between FL and FL-3A may be due to substitutions of serine with alanine, though Myc-Otx2-ΔAD and ΔAD-3A migrated similarly (see Fig. 1D). Calculated and apparent molecular masses of constructs (kDa) were 43 and 50 for Myc-Otx2FL, 22 and 30 for Myc-Otx2-HD, 32 and 40 for Myc-Otx2ΔAD, 23 and 35 for Myc-Otx2-AD, and 34 and 50 for Myc-Otx2ΔRD, respectively. Black circles, undesired products or degradation products; orange arrowheads, bands resistant to λ-PP, which may correspond to an upper band of ΔRD in panel A.

Development • Supplementary information

Fig. S2 (Satou et al.)

Development • Supplementary information

Fig. S2 (Satou et al.)

Fig. S2. Alignment of amino acid sequences of Otx2 and Otx5/Crx among vertebrates.
Abbreviations of species are *Xenopus laevis* (Xl), *Xenopus tropicalis* (Xt), *Danio rerio* (Dr), *Gallus gallus* (Gg), *Mus musculus* (Mm) and *Homo sapiens* (Hs). Protein sequences were obtained from the NCBI database: Xl_Otx2.L (NP_001084955), Xl_Otx5.L (NP_001081916), Xt_Otx2 (NP_001016177), Xt_Otx5 (NP_001016021), Dr_Otx2 (NP_571326), Dr_Otx5 (NP_851848), Gg_Otx2 (NP_989851), Gg_Otx5 (NP_001288716), Mm_Otx2 (NP_001273412), Mm_Crx (NP_031796), Hs_Otx2 (NP_001257453), Hs_Crx (AAH53672). Boxes coloured in green, homeodomain; blue, SIWSPAS motif; yellow, repeated Otx tail motif; red, Otx2 mutation sites (P133 and P134) that were reportedly associated with human ocular malformation. Blue or magenta letters, consensus motifs for Akt and Cdks. Bold cases, putative phosphorylation sites of Otx2 as shown in this study.

Development • Supplementary information

Fig. S3 (Satou et al.)

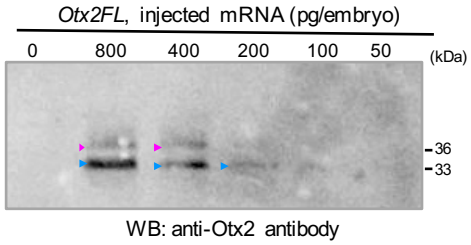

Fig. S3. The detection limit of Otx2FL by western blotting.
Embryos were injected with *Otx2FL* mRNA at various doses as indicated. Modified bands of Otx2FL was clearly detected when *Otx2FL* mRNAs were injected at higher than 200 pg per embryo. Embryonic lysate of 0.42 equivalent embryo was loaded per lane. Otx2FL was detected by western blotting with anti-Otx2 antibodies. Blue arrowheads, nascent protein; magenta arrowheads, modified proteins.

Development • Supplementary information

Fig. S4 (Satou et al.)

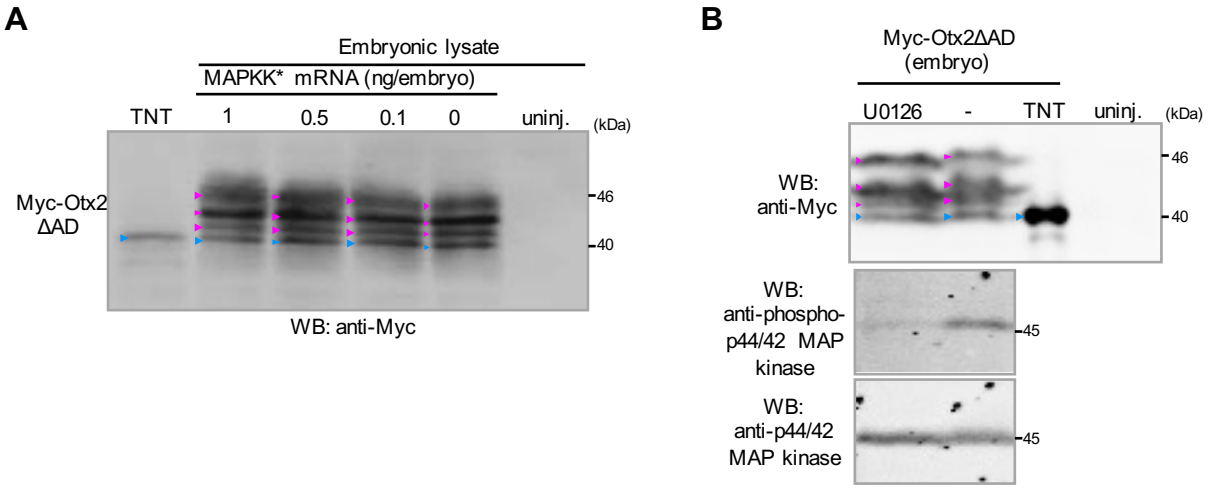

Fig. S4. Effect of MAPK on modifications of Otx2.
(A) No effect of a constitutively active mutant of MAPKK (MAPKK*) on modifications of Otx2. Overexpression of MAPKK* did not apparently affect the modified bands of Myc-Otx2ΔAD even with the high-dose injection of MAPKK *. The amounts of injected *MAPKK*** mRNA were as indicated. mRNAs were injected into the animal pole region of both blastomeres at the 2-cell stage. (B) No effect of the chemical inhibitor for MEK (MAPKK), U0126, on modifications of Otx2. Myc-Otx2ΔAD expressing embryos were injected with U0126 into the blastocoel at the early blastula (stage 6), and subjected at the gastrula (stage 10.5) to western blotting with anti-Myc, anti-p44/42 MAP kinase and anti-phospho-p44/42 MAP kinase antibodies as indicated. Blastocoel injection of U0126, which reduced the activation form of MAPK, phospho-p44/42 MAP kinase (Fig. S4B, middle and bottom panels), did not affect the modified bands of Myc-Otx2ΔAD (upper panel). Blue arrowheads, nascent proteins; magenta arrowheads, modified proteins.

Development • Supplementary information

Fig. S5 (Satou et al.)

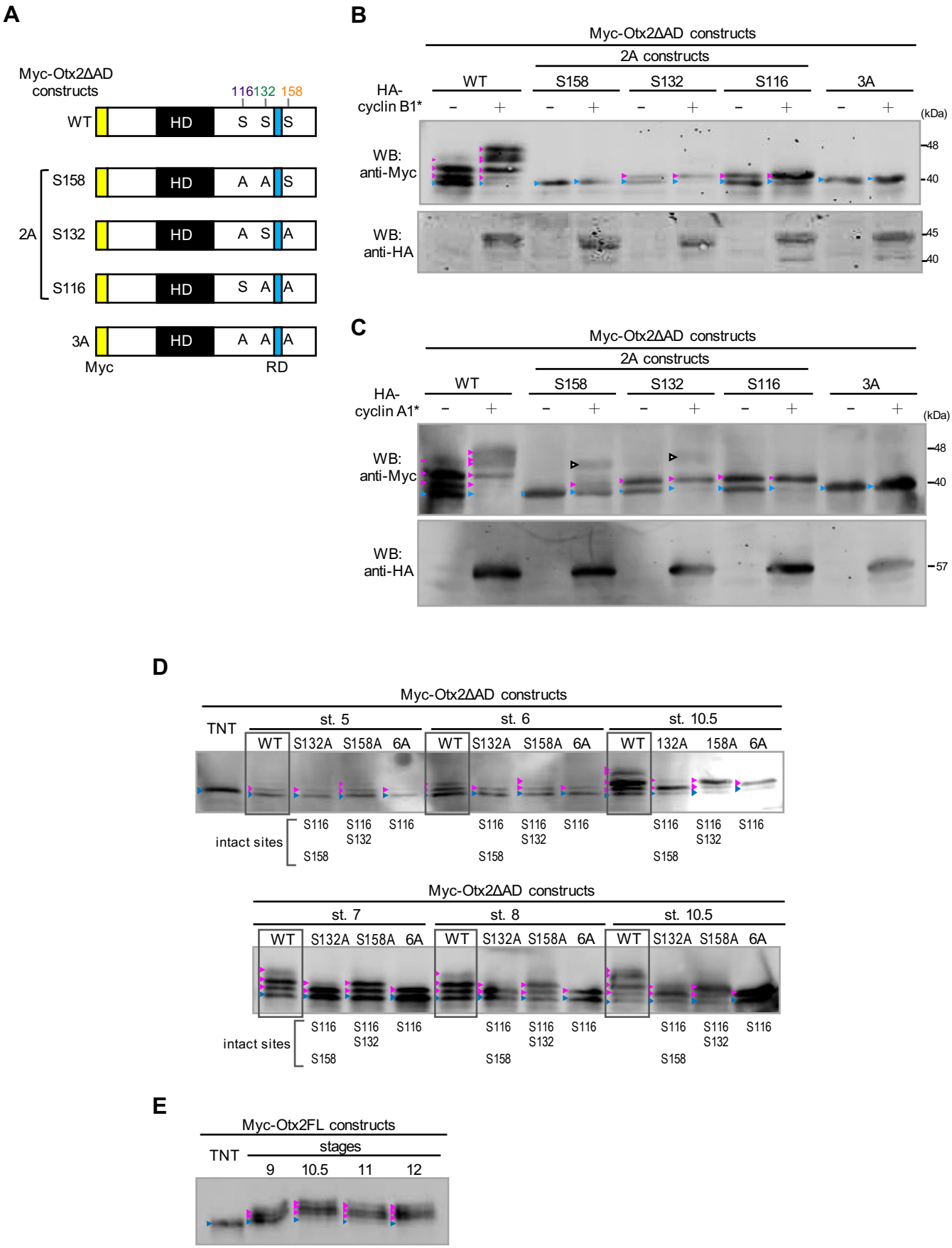

Development • Supplementary information

Fig. S5. Preference of cyclin B/Cdk and cyclin A/Cdk for C-sites of Otx2.
(A) Schematic presentation of Myc-Otx2ΔAD with double (2A) and triple alanine (3A) mutations at S116, S132 and S158. To test a preference of cyclin B/Cdk and cyclin A/Cdks for Otx2 phosphorylation, double alanine mutants (2A) for S116, S132 and S158 in ΔAD were constructed, in which only one site is responsible for Otx2 phosphorylation. In the 2A constructs, for example, the S158 construct indicates mutations at S116 and S132. Yellow box, Myc-tag; black box, homeodomain (HD); blue box, repression domain (RD). S, serine phosphorylation sites (S116, S132, S158); A, alanine mutation. (B) Western blotting of Myc-Otx2ΔAD constructs (2A or 3A) co-expressed with (+) or without (-) HA-cyclin B1*. The intensity of modified bands of S132 (S116A/S158A) and S116 (S132A/S158A) constructs, but not that of S158 (S116A/S132A), was increased by HA-cyclin B1* expression. (C) Western blotting of Myc-Otx2ΔAD constructs (2A or 3A) co-expressed with (+) or without (-) HA-cyclin A1*. All modified bands were enhanced by HA-cyclin A1* expression, with an additional modified band (white arrowheads). These data suggest that S116 and S132 have a preference for both cyclin B/Cdk and cyclin A/Cdks, and that S158 has it for cyclin A/Cdks, if Otx2 is directly phosphorylated by cyclin/Cdks. (D,E) Developmental changes of phosphorylation of Otx2 as assayed by using Myc-Otx2ΔAD (D) and Myc-Otx2FL (E) constructs. The wild type (WT) and alanine mutants of a single serine at S132 (S132A) and S158 (S158A), and of 6 serines at S122, S123, S132, S153, S158, and S161 (6A) in Myc-Otx2ΔAD constructs were analyzed from stages 5 to 10.5 as indicated. Note that the 6A construct has S116, which is a phosphorylation site. Mutation at S132 (S132A and 6A constructs) reduced phosphorylation levels compared to S158 mutation, indicating that S132 and S116 are more efficiently phosphorylated than S158 during cleavage stages. Myc-Otx2FL was analyzed at stages 9 to 12 as indicated. TNT, *in vitro* translation products; blue arrowheads, nascent bands; magenta arrowheads, modified bands. Blue arrowheads, nascent proteins; magenta arrowheads, modified proteins; white arrowheads, additional modified bands at sites other than S116, S132 and S158.

Development • Supplementary information

Fig. S6 (Satou et al.)

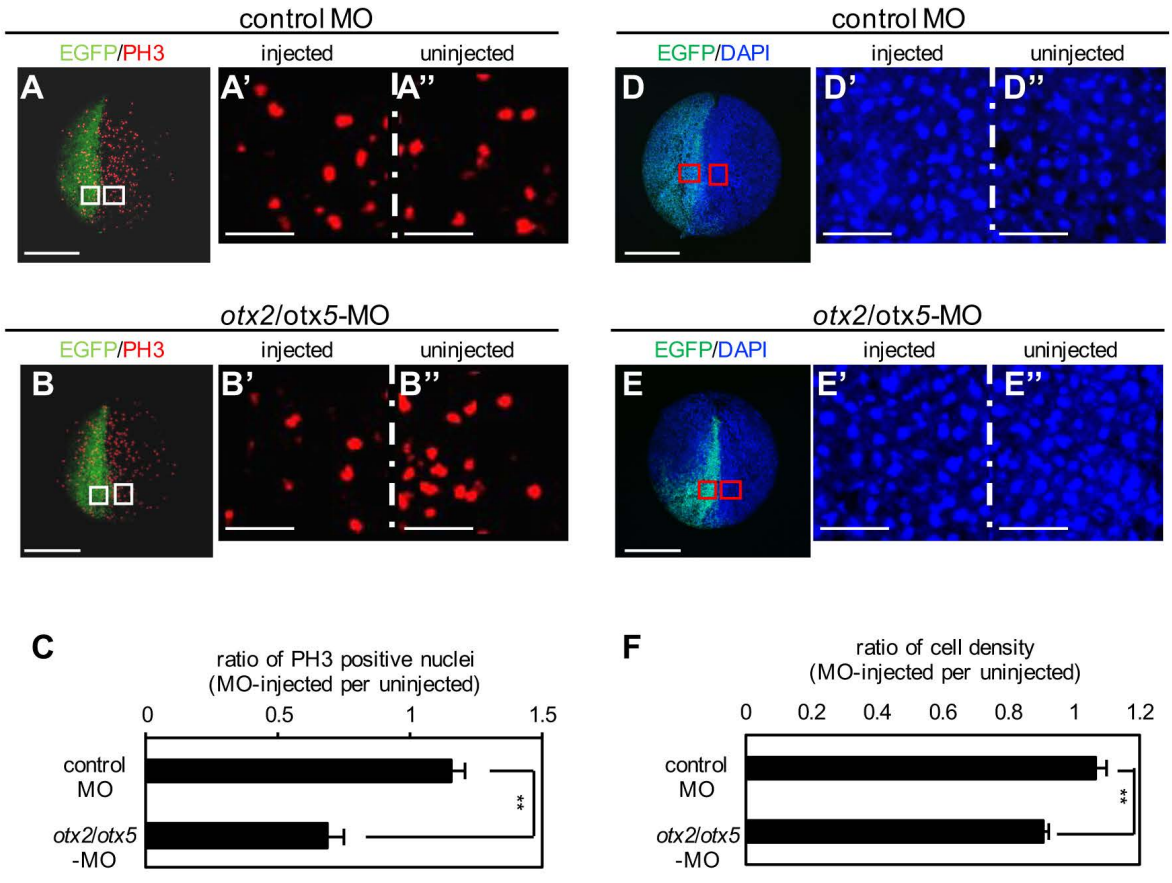

Fig. S6. Reduction of cell proliferation by *otx2/otx5* knockdown in *X. tropicalis* embryos.
Knockdown experiments were performed using *X. tropicalis*. Previous study using MO-injection in *X. tropicalis* embryos has shown that Otx2 and its paralogue Otx5, which are expressed in anterior neuroectoderm, have functional redundancy in head development (Yasuoka et al., 2014). *X. tropicalis* is a diploid species closely related to the tetraploid species *X. laevis* and suitable for MO knockdown experiments, and all three C-sites of Otx2 are conserved in Otx5 (Fig. S2). MOs together with FITC dextran as a tracer were injected into one blastomere at the 4-cell stage of *X. tropicalis* embryos; followed by PH3 immunostaining and DAPI staining at early neural stage. PH3 immunostaining, DAPI nuclear staining were the same as in Fig. 5. The numbers of stained nuclei were counted and compared between injected and uninjected areas. (A,B) Effects of *otx2/otx5*-MO injection on mitotically active cells. White boxes, enlarged area (A'-B"). (C) Quantitative analysis for the ratio of PH3-positive nuclei. PH3-positive nuclei in an injected or uninjected area (0.072 mm^2) in each embryo were counted (more than 60 nuclei in each area) with 9 embryos, and the ratio of the numbers of injected versus uninjected area was calculated for each embryo to obtain mean ± s.e.m. from 9 embryos. The ratio of PH3-positive nuclei in control MO-injected embryos was 1.15 ± 0.055 (mean ± s.e.m.), whereas that in *otx2/otx5*-MOs-injected embryos was 0.688±0.063, which significantly differed from the control (p = 4.95E-05). (D,E) Effects of *otx2/otx5*-MO on cell density. Red boxes, enlarged area (D'-E"). (F) Quantitative analysis for the ratio of cell densities. More than 500 total nuclei in each area (0.072 mm^2) were counted in one embryo, and 9 embryos were analysed. The ratio of cell density in control MO-injected embryos was 1.063 ± 0.034 (mean ± s.e.m.), whereas that in *otx2/otx5*-MOs-injected embryos was 0.906 ± 0.013, which differed from the control (p = 0.0015). **P<0.01 (t-test); error bars, s.e.m. (C,F). Scale bar, 500 µm (A,B,D,E); 50 µm (A'-B",D'-E",). The amount of injected MO (pmol/embryo): control MO, 1; *otx2/otx5*, 0.5 each.

Development • Supplementary information

Fig. S7 (Satou et al.)

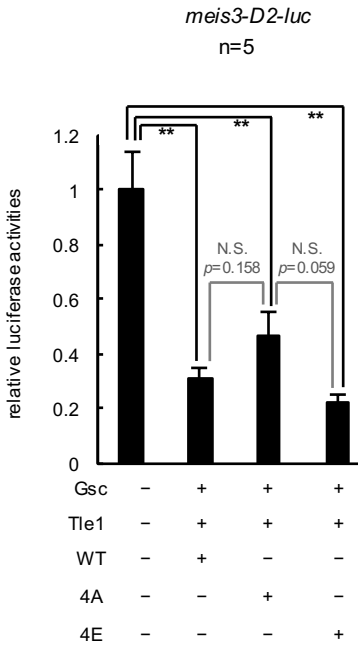

Fig. S7. Repression activity of Otx2-4A and -4E together with Gsc and Tle1.
Experimental procedures were the same as Fig. 7L. Repression activity of Otx2-4A requires Gsc for *meis3-D2-luc* reporter. *meis3-D2-luc* reporter DNA was co-injected with mRNAs for Gsc (12.5 pg/embryo), Tle1 (12.5 pg/embryo), Otx2-WT, or -4A (25 pg/embryo), or 4E (25 pg/embryo) as indicated. $^{**}P<0.01$ (t-test); error bars, s.e.m.; N.S., not significant; n, the number of samples.

Development • Supplementary information

Table S1. The list of plasmid constructs made in this study

Plasmid names	Cloning sites	Vectors	Comments
pCSf107_MycOtx2FL_T	*Bam*HI, *Xba*I	pCSf107_MTmT	aa 1-288 (Full length: FL) Otx2. S (*X. laevis*) NP_001084160
pCSf107_MycOtx2HD_T	*Bam*HI, *Xba*I	pCSf107_MTmT	aa 1-96
pCSf107_MycOtx2ΔAD_T	*Bam*HI, *Xba*I	pCSf107_MTmT	aa 1-184
pCSf107_MycOtx2AD_T	*Bam*HI, *Xba*I	pCSf107_MTmT	aa 185-288
pCSf107_MycOtx2ΔRD_T	*Bam*HI, *Xba*I	pCSf107_MTmT	aa 1-96/185-288
pCSf107_MycOtx2ΔAD-S116A_T	*Bam*HI, *Xba*I	pCSf107_MTmT	
pCSf107_MycOtx2ΔAD-S122A_T	*Bam*HI, *Xba*I	pCSf107_MTmT	
pCSf107_MycOtx2ΔAD-S123A_T	*Bam*HI, *Xba*I	pCSf107_MTmT	
pCSf107_MycOtx2ΔAD-S132A_T	*Bam*HI, *Xba*I	pCSf107_MTmT	
pCSf107_MycOtx2ΔAD-S153A_T	*Bam*HI, *Xba*I	pCSf107_MTmT	
pCSf107_MycOtx2ΔAD-S158A_T	*Bam*HI, *Xba*I	pCSf107_MTmT	
pCSf107_MycOtx2ΔAD-S161A_T	*Bam*HI, *Xba*I	pCSf107_MTmT	
pCSf107_MycOtx2ΔAD-3A_T	*Bam*HI, *Xba*I	pCSf107_MTmT	S116A, S132A, S158A
pCSf107_MycOtx2ΔAD-4A_T	*Bam*HI, *Xba*I	pCSf107_MTmT	T115A, S116A, S132A, S158A
pCSf107_MycOtx2ΔAD-2A(S158)_T	*Bam*HI, *Xba*I	pCSf107_MTmT	S116A, S132A
pCSf107_MycOtx2ΔAD-2A(S132)_T	*Bam*HI, *Xba*I	pCSf107_MTmT	S116A, S158A
pCSf107_MycOtx2ΔAD-2A(S116)_T	*Bam*HI, *Xba*I	pCSf107_MTmT	S132A, S158A
pCSf107_Otx2-WT_T	*Bam*HI, *Xba*I	pCSf107_mT	Wild type: WT
pCSf107_Otx2-4E_T	*Bam*HI, *Xba*I	pCSf107_mT	T115E, S116D, S132E, S158E
pCSf107_Otx2-T115A_T	*Bam*HI, *Xba*I	pCSf107_mT	
pCSf107_Otx2-3A_T	*Bam*HI, *Xba*I	pCSf107_mT	S116A, S132A, S158A
pCSf107_Otx2-4A_T	*Bam*HI, *Xba*I	pCSf107_mT	T115A, S116A, S132A, S158A
pCSf107_Otx2-A2A(S116)_T	*Bam*HI, *Xba*I	pCSf107_mT	T115A, S132A, S158A
pCSf107_Otx2-A2A(S132)_T	*Bam*HI, *Xba*I	pCSf107_mT	T115A, S116A, S158A
pCSf107_Otx2-A2A(S158)_T	*Bam*HI, *Xba*I	pCSf107_mT	T115A, S116A, S132A
pCSf107_Otx2ΔAD-4A_T	*Bam*HI, *Xba*I	pCSf107_mT	
pCSf107_Otx2ΔAD-4E_T	*Bam*HI, *Xba*I	pCSf107_mT	
pCSf107_HA-cyclin A1*_T	*Bam*HI, *Xho*I	pCSf107_4HAmT	replaced Δcyclin A1 (from Dr. N. Furuno)
pCSf107_HA-cyclin B1*_T	*Bam*HI, *Eco*RI	pCSf107_4HAmT	replaced GST-ΔN106cyclin B1 (Iwabuchi et al., 2002)
pCSf107_p27xic1_T	*Bam*HI, *Xho*I	pCSf107_mT	
pCSf107_HATLE1_T	*Age*I, *Xba*I	pCSf107_4HAmT	Replaced pCSf107-TLE1 (Yasuoka et al., 2014)
pCSf107_pax6_T	*Sfu*I, *Not*I	pCSf107_mT	replaced pCS105-pax6

Note: the postfix "_T" indicates the presence of SP6/T7 terminators at the end of the transcribed region.

Development • Supplementary information

Table S2. The list of cutting sites and RNA polymerases for the in vitro transcription of anti-sense RNA probe

Plasmid names	Cutting sites	RNA polymerase	Comments
pCSf107_p27xic1_T	*BamHI*	T7	
pCSf107_ Otx2-WT_T	*BamHI*	T7	
pBS SK(-)gbx2	*EcoR*I	T3	
pBSK_xcg1	*NotI*	T3	
pCS107BSX_rax	*Xho*I	SP6	
pCSf107_pax6_T	*Sal*I	T7	
BS4A 3(X pax2-2a)	*EcoR*I	T3	(Takada et al., 2005)

References

Takada, H., Hattori, D., Kitayama, A., Ueno, N. and Taira, M. (2005). Identification of target genes for the Xenopus Hes-related protein XHR1, a prepattern factor specifying the midbrain-hindbrain boundary. *Dev. Biol.* **283**, 253–267.

Development • Supplementary information